PAT1-type GRAS-domain proteins control regeneration by transcriptional activation of *DOF3.4* driving cell proliferation

Anchal Bisht,[1,2] Thomas Eekhout,[1,2] Balkan Canher,[1,2] Ran Lu,[1,2] Ilse Vercauteren,[1,2] Geert De Jaeger,[1,2] Jefri Heyman[1,2,†] and Lieven De Veylder,[1,2,*,†]

[1]Department of Plant Biotechnology and Bioinformatics, Ghent University, Ghent, B-9052, Belgium

[2]Center for Plant Systems Biology, VIB, Ghent, B-9052, Belgium

[*] Author for correspondence: lieven.deveylder@psb.vib-ugent.be

[†] Senior authors

A.B., J.H. and L.D.V. conceived and designed the research. A.B., J.H., B.C., R.L. and I.V. performed the experiments. A.B., J.H., T.E, G.D.J. and L.D.V analyzed data. A.B., J.H. and L.D.V. wrote the article. All authors read, revised, and approved the article.

The author responsible for distribution of materials integral to the findings presented in this article in accordance with the policy described in the Instructions for Authors (https://academic.oup.com/plcell) is: Lieven De Veylder (lieven.deveylder@psb.vib-ugent.be).

ORCID IDs: 0000-0003-4290-6647 (A.B.); 0000-0003-3266-4189 (J.H.); 0000-0002-2878-1553 (T.E.); 0000-0001-5118-4178 (B.C.); 0000-0002-2536-1692 (R.L.); 0000-0001-9561-8468 (I.V.); 0000-0001-6558-5669 (G.D.J.); 0000-0003-1150-4426 (L.D.V.)

SHORT TITLE: PAT1-type GRAS proteins drive regeneration

ONE-SENTENCE SUMMARY: PAT1-type GRAS transcription factors redundantly control root regeneration by activating DOF3.4 driving D-type cyclin expression.

CORRESPONDING AUTHOR:

Lieven De Veylder

Center for Plant Systems Biology

VIB-Ghent University

Technologiepark 71, B-9052 Gent (Belgium).

Tel.: +32 9 3313800; Fax: +32 9 3313809; E-mail: lieven.deveylder@psb.vib-ugent.be

Abstract

Plant roots possess a remarkable regenerative potential owing to their ability to replenish damaged or lost stem cells. The ETHYLENE RESPONSE FACTOR 115 (ERF115), one of the key molecular elements that have been linked to this potential, plays a predominant role in the activation of regenerative cell divisions. However, the downstream operating molecular machinery driving wound-activated cell division is largely unknown. Here, we biochemically and genetically identified the GRAS-domain transcription factor SCARECROW-LIKE 5 (SCL5) as an interaction partner of ERF115. Although being non-essential under control growth conditions, SCL5 controls redundantly with the related PHYTOCHROME A SIGNAL TRANSDUCTION 1 (PAT1) and SCL21 transcription factors the expression of the *DNA-BINDING ONE FINGER 3.4* (*DOF3.4*) transcription factor gene. *DOF3.4* expression is wound-inducible in an ERF115-dependent manner, and in turn activates D3-type cyclin expression. Accordingly, ectopic *DOF3.4* expression drives periclinal cell division, while its downstream D3-type cyclins are essential for regeneration of a damaged root. Our data highlight the importance and redundant role of the SCL5, SCL21 and PAT1 transcription factors in the process of wound-activated regeneration processes and pinpoint the DOF3.4 as a key downstream element driving regenerative cell division.

Introduction

Regeneration is the process by which a tissue or organ regains its complete structure and function after injury, representing a self-preservation mechanism. Depending on the species, the extent of regeneration is highly variable. Vertebrates can regenerate certain structures, such as limbs in salamanders or tail fins in fish. In humans, there are anecdotal reports of digit regeneration after amputation of fingertips (Illingworth, 1974). Invertebrate species, including sea squirts, planarian flatworms, and cnidarians, are capable of more extensive tissue replacement (Ricci and Srivastava, 2018). No clade, however, competes with plants that are known for their unparalleled regenerative capacity, allowing them to regenerate for survival under severe stress conditions, such as herbivory attack and harsh weather conditions. This regeneration potential is exemplified in Arabidopsis (*Arabidopsis thaliana*), where a completely excised root tip is efficiently regenerated within three to four days (Sena et al., 2009). Remarkably, plant regeneration not only replenishes tissues and restores damaged organs but can also give rise to whole plant bodies (Ikeuchi et al., 2019; Christiaens et al., 2021). This unique feature of asexual reproduction is widely exploited in modern agricultural applications, including vegetative propagation and grafting (Sussex, 2008; Duclercq et al., 2011; Xu and Huang, 2014).

One critical feature of plant regeneration is the reformation and maintenance of meristems, the proliferative tissues that hold the stem cells. Like animal stem cells, plant stem cells are defined by their ability to renew themselves and to generate daughter cells that establish tissues and organs. These stem cells are maintained in specialized microenvironments, commonly referred to as stem cell niches (SCN). Within Arabidopsis, the SCN holds a quiescent center (QC) that is surrounded by a single tier of stem cells (van den Berg et al., 1997; Sarkar et al., 2007). Despite their low proliferation rate, QC cells have been found to operate as "reservoir" to provide new cells. When stress occurs, QC cells are triggered to divide and contribute to lost neighboring stem cells, a process driven by many different signals, including hormones like auxin, cytokinin, brassinosteroids, ethylene, and jasmonate (Aida et al., 2004; Curtis and Hays, 2007; Fulcher and Sablowski, 2009; Cruz-Ramírez et al., 2013; Mähönen et al., 2014; Zhou et al., 2019; Lu et al., 2021). Within the QC, *WUSCHEL-RELATED HOMEOBOX 5* (*WOX5*) gene expression is required to maintain QC cell identity (Sarkar et al., 2007).

Previously, we have identified within Arabidopsis the ETHYLENE RESPONSE FACTOR 115 (ERF115) transcription factor that controls the replenishment of lost cells or tissues within the root meristem following wounding (Heyman et al., 2013; Heyman et al.,

2016). *ERF115* expression is instantly induced in cells adjacent to cells that undergo cell death, such as induced by root tip excision, selective killing of stem cells by cytotoxic drugs or laser-mediated cell ablation (Heyman et al., 2016; Marhava et al., 2019; Zhou et al., 2019; Hoermayer et al., 2020). Activated ERF115 subsequently facilitates the reprograming of these cells to become the new stem cells. These cells consequently undergo formative cell division, generating cells that replenish the damaged ones (Heyman et al., 2016; Canher et al., 2020; Hoermayer et al., 2020). Strikingly, even as little as a single dying cell activates a rapid *ERF115* response in its surrounding cells. During recovery from laser-assisted root stem cell removal, ERF115 was found to interact biochemically and genetically with the RETINOBLASTOMA RELATED – SCARECROW (RBR – SCR) signaling network that controls stem cell divisions in response to environmental stress (Zhou et al., 2019).

Once activated, ERF115 acts as a transcriptional activator of the *PHYTOSULFOKINE 5* (*PSK5*) precursor gene (Heyman et al., 2013), encoding a small peptide hormone known for its cell division-promoting potential in suspension cultures and QC cells (Matsubayashi and Sakagami, 1996; Kong et al., 2018). In addition, ERF115 controls expression of the *WOUND INDUCED DEDIFFERENTIATION 1* transcription factor gene (Heyman et al., 2016), facilitating the reprograming of cells and hence allowing them to regain pluripotency required to initiate tissue regeneration (Iwase et al., 2011). Furthermore, ERF115 enhances auxin sensitivity in wound-adjacent cells through transcriptional activation of the *MONOPTEROS/AUXIN RESPONSE FACTOR 5* (*MP/ARF5*) gene, thereby triggering the reacquisition of stem cell identity (Canher et al., 2020). Contrastingly, the molecular components that link ERF115 with the cell cycle machinery are still unknown.

Next to ERF115, GIBBERELLIN-INSENSITIVE, REPRESSOR of ga1-3, SCARECROW (GRAS)-domain transcription factors may play a role in the regeneration process. The GRAS-domain protein family holds eight subfamilies that act in a diverse set of stress and developmental processes (Tian et al., 2004). Among these, the members of the DELLA family act as repressors of the gibberellin signaling pathway (Cheng et al., 2004; Cao et al., 2005), whereas HAIRY MERISTEM (HAM) proteins are essential for indeterminate growth maintenance, with *ham* mutants displaying a shoot meristem arrest and differentiation phenotype (Engstrom, 2012). SHORT ROOT (SHR) and SCR are involved in the control of root radial patterning and root growth (Helariutta et al., 2000). The Arabidopsis PHYTOCHROME A SIGNAL TRANSDUCTION 1 (PAT1) subfamily holds five genes, namely *PAT1, SCL1, SCL5, SCL13* and *SCL21* (Bolle, 2004). Among these, *PAT1* and its closest homolog *SCL21* were originally identified as components that act positively on the

phytochrome A (phyA)-dependent light signaling pathway (Bolle, 2004; Torres-Galea et al., 2006; Torres-Galea et al., 2013). Additionally, the PAT1 protein dimerizes with ERF115 to boast its regenerative potential, because ectopic coexpression of Arabidopsis *ERF115* with *PAT1* activates neoplastic growth that manifests itself by spontaneous callus formation (Heyman et al., 2016). Correspondingly, the *erf115* and *pat1* single and double mutants show an equally impaired root tip regeneration phenotype, suggesting that these two proteins form an active protein complex rather than acting in two independent pathways.

ERF115 belongs to the EREB-DREB subfamily X of the AP2/ERF group of transcription factors, comprising eight members, namely *ERF108* to *ERF115* (Heyman et al., 2018). Sequence alignment of the EREB-DREB subfamily X revealed a conserved 11-amino-acid (AA) CMX-1 motif in the N-terminal region as a common feature of all members but ERF112 (Nakano et al., 2006). This motif was found to be both essential and sufficient to drive interaction with the PAT1-related SCL21 transcription factor (Heyman et al., 2016). Here, through a systematic interaction study between all EREB-DREB subfamily X and PAT1 subfamily members, we identified SCL5 as a novel interaction partner of ERF115. SCL5 operates redundantly with its family members PAT1 and SCL21 in the reconstitution of the SCN following wounding. Moreover, we demonstrate that SCL5, along with PAT1 and SCL21, drives regenerative cell division through the transcriptional control of *DNA-BINDING ONE FINGER 3.4* (*DOF3.4*, also known as *OBP1*), which in turn activates the expression of cyclin *CYCD3;3*.

Results

SCL5 is an interactor of ERF114 and ERF115

Although ectopic coexpression of *ERF115* and *PAT1* was found to dramatically boost the regenerative capacities of ERF115, the corresponding *erf115 pat1* double mutant failed to mimic the complete loss of regeneration phenotypes that were observed for plants expressing the dominant-negative $ERF115^{SRDX}$ allele, suggesting redundancy with putative additional ERF-GRAS heterodimers. To gain insight into the possible pairwise interactions between the subfamily X of EREB-DREB transcription factors and the GRAS-domain protein subgroup PAT1 family, a yeast two-hybrid (Y2H) strategy was followed. In this assay, SCL13 showed a strong autoactivation, whereas SCL1 failed to show interaction with any of the tested ERF members (Figure 1A and B). PAT1 interacted with five ERF members (all except ERF108, ERF112, and ERF113), whereas SCL21 was found to interact with all members except ERF112, fitting with the absence of the N-terminally located 11-AA CMX-1 motif demonstrated before

to mediate interaction with SCL21 (Heyman et al., 2016). SCL5 interacted with four ERF proteins, namely ERF109, ERF111, ERF114 and ERF115.

Previously, SCL5 could not be detected in a tandem affinity purification experiment using ERF115 as protein bait (Heyman et al., 2016), possibly due to only a transient interaction between SCL5 and ERF115. Therefore, an ERF115 single-step affinity purification followed by mass spectrometry was performed, increasing the chance to identify loose and/or transient interaction partners. Next to ERF113 and ERF114, both SCL21 and SCL5 could be detected amongst the ERF115 copurifying proteins (Table 1; Supplemental Dataset S1), confirming the interaction between SCL5 and ERF115 at the biochemical level.

To study putative coexpression with *ERF115*, available gene annotation data was used to construct an *SCL5* transcriptional reporter line. Using 2,587 bp of the predicted sequence upstream of the *SCL5*-coding region, independent reporter lines driving the expression of a nuclear-targeted GFP were generated, revealing a weak GFP-positive signal within cortical and endodermal meristem cells and a stronger signal in a subset of the vascular stem cells (Supplemental Figure S1A). However, these reporter lines did not show the expected nuclear-localized GFP signal, suggesting that the predicted promoter region might be incorrect. Therefore, we remapped *SCL5* RNA-sequencing (RNA-seq) reads on the genomic locus, revealing the absence of detectable reads matching the beginning of the first predicted *SCL5* exon (Supplemental Figure S1C), suggesting a misannotation of the *SCL5* start of translation site. The next in-frame start codon is located 569 bp downstream of the annotated start codon (Supplemental Figure S1D), resulting in an open reading frame (ORF) of 1,581 bp, encoding a 526-AA long protein. This prediction is supported by the Arabidopsis PeptideAtlas (www.peptideatlas.org/builds/arabidopsis) that maps all available mass spectrometry peptide data (van Wijk et al., 2021). The newly predicted *SCL5* ORF was retested in the Y2H assay. Although the new SCL5 encoded protein could not be used as bait due to autoactivation, it could be used as a prey against ERF fragment baits holding the N-terminal GRAS-domain interaction motif, resulting in an interaction with the same ERF members as found before (Figure 1C and D). In addition, a bimolecular fluorescence complementation experiment using the ERF115-headGFP and SCL5-tailGFP protein fusions revealed a clear restoration of GFP fluorescence in the nucleus of *Nicotiana benthamiana* pavement cells, indicative for *in vivo* ERF115-SCL5 association (Supplemental Figure S2A), a pattern similar to the previously reported ERF115 and SCL21 interaction (Heyman et al., 2016) (Supplemental Figure S2B), opposed to its negative controls (Supplemental Figure S2C and S2D).

Supported by these observations, new *SCL5* promoter reporter lines were generated using the reannotated 2,525-bp promoter sequence, revealing *SCL5* expression throughout the root meristem displaying the characteristic nuclear-localized signal, with an apparently stronger expression in the SCN, as well as the stele, pericycle, and endodermal tissue (Supplemental Figure S1B), a pattern substantiated by available single cell RNA-seq data (https://rootcellatlas.org). Following treatment with bleomycin to induce vascular stem cell death and subsequent *ERF115* expression, a substantial overlap between the *SCL5* and *ERF115* expression patterns could be observed (Figure 1E, Supplementary Figure S3), supporting the potential *in planta* interaction between the two gene products.

Ectopic ERF-GRAS expression results in neoplasm in both root and shoot

To find support for a genetic interaction between *SCL5* and *ERF115*, as well as its closest relative *ERF114*, we phenotypically compared single versus *ERF-GRAS* co-overexpressing plants. Within these experiments, *PAT1* and *SCL21* were taken along as a positive controls. Young seedlings with ectopic overexpression of *ERF115* and *SCL21* displayed a significant reduction in root length compared with the wild type, in accordance with previous observations (Heyman et al., 2016; Lu et al., 2021) (Figure 2A, Supplemental Figure S4). At the microscopic level, only overexpression of *SCL21* appeared to cause a significant reduction in the number of meristematic cortex cells compared with the wild type (Supplemental Figure S5). Subsequently, we phenotypically analyzed the offspring obtained from crosses between these different lines. Co-overexpression of *ERF115* with *SCL5*, *SCL21*, or *PAT1* resulted in a strong inhibition of root growth compared with the single overexpression lines (Figure 2A; Supplemental Figure S4), which correlated with a disorganized SCN (Figure 2B), callus formation at the root–hypocotyl junction, and a disorganized shoot (Figure 2C), as was reported before for *ERF115-PAT1* co-overexpressing plants (Heyman et al., 2016). When testing the genetic interaction with *ERF114*, effects on primary root growth were less outspoken compared to *ERF115* interaction (Supplemental Figure S4 and S6A). Likewise, a disorganized root SCN was detected for all respective combinations (Supplemental Figure S6B), although less pronounced as compared with the *ERF115* combinations (Figure 2B), whereas the disorganized shoot phenotypes were much alike (Supplemental Figure S6C). Following 25 days of growth, $ERF114^{OE}$ plants displayed the previously reported increased bud outgrowth (Mehrnia et al., 2013), whereas $SCL21^{OE}$ plants showed a reduction in rosette size (Supplemental Figure S7). For the different ERF-GRAS co-overexpressing combinations, distinct phenotypic responses were observed (Supplemental Figure S7), of which the severity varied. Overall, these data demonstrate that

ERF114 and *ERF115* in combination with *SCL5, PAT1,* or *SCL21* trigger phenotypes that affect meristem activity. The synergetic effect of both transcription factor classes was confirmed for the *ERF115*-related crosses at the level of *PSK5* expression, a previously reported ERF115 target gene (Figure 2D).

The GRAS-domain *scl5 pat1 scl21* triple mutant is regeneration deficient

Single mutants of *pat1* were reported to show only a mild defect on root regeneration post wounding (Heyman et al., 2016), probably owing to gene redundancy. Therefore, we generated *scl5 scl21, scl5 pat1* and *pat1 scl21* double mutants and the *scl5 scl21 pat1* triple mutant. Under control conditions, even the *scl5 scl21 pat1* triple mutant did not show any clear macroscopic difference compared with wild-type (Col-0) plants (Supplemental Figure S8). Subsequently, these mutant combinations were tested for a putative wound-responsive phenotype. After a 24-h bleomycin treatment that results in vascular cell death, the roots were transferred to bleomycin-free medium, allowing them to replenish the dead cells through regenerative cell divisions (Heyman et al., 2013; Canher et al., 2020). Following five days of recovery, the regeneration rate was slightly, but significantly, reduced for the *pat1 scl5* and *pat1 scl21* double mutant combinations, whereas the triple *scl5 scl21 pat1* mutant displayed a strong impairment in regeneration capacity (Figure 3A). This phenotype could be complemented by the introduction of a *pSCL5:SCL5-GFP* or *pPAT1:PAT1-GFP* translational reporter line (Figure 3B), confirming that the combinational absence of the three GRAS proteins accounted for the regeneration defective phenotype.

The bleomycin regeneration-deficient phenotype was studied at the cellular level using the *WOX5* QC cell identity marker, demonstrated before to accumulate in an ERF115-dependent manner in the endodermal and vascular cells neighboring the dead cells (Heyman et al., 2013; Canher et al., 2020). To this end, the *pWOX5:NLS-GFP/GUS* construct was introduced in the *scl5 scl21 pat1* triple mutant by a new transformation event. Under control conditions and following 24 h of bleomycin treatment, no clear differences in the *WOX5-GFP* expression pattern between wild-type and *scl5 scl21 pat1* triple mutant plants could be observed (Figure 3, E and F). In Col-0 plants, upon retransfer of the bleomycin-treated plants to drug-free medium, the *WOX5-GFP* expression domain increased shootwards and infiltrated the vascular tissue that surrounded the damaged cells (Figure 3E). Eventually, the *WOX5-GFP* signal was reconfined to the SCN three days post transfer, which coincided with the recovery of the root tip visualized by the strong reduction in cell death, demonstrated before to be in part due to periclinal endodermal cell divisions (Canher et al., 2020). By contrast, within the *scl5*

scl21 pat1 mutant roots, the *WOX5-GFP* accumulation pattern appeared to diminish during the 24 h-48 h post recovery timeframe, followed by a collapse of the vascular tissue at 72 h (Figure 3F), probably accounting for the arrest in root growth (Figure 3A). These data indicate that the three GRAS transcription factors are required for meristem reestablishment following vascular stem cell death, likely by participating in the periclinal divisions demonstrated before to replenish the vascular cells.

Next, we tested the regenerative response of the *scl5 scl21 pat1* mutant following root tip excision. Whereas 55% of the control plants were able to generate a new root tip following removal of the 200-µm distal portion within three days, the regeneration rate dropped to less than 2% in the triple mutant (Figure 3C). Likewise, the regenerative response of the triple mutant towards laser-mediated cell ablation was investigated, where single cells were killed in a cell type-specific manner. Single cell wounding typically involves a change in division plane from anticlinal (perpendicular to the growth axis) to periclinal (parallel to the growth axis) in cells located adjacent to the damaged cell in the inward located cell file, allowing for efficient replacement of the dead cells (Marhava et al., 2019). Compared with the wild type, a significant decrease in periclinal division potential in the adjacent cortex or endodermal cells could be observed within the *scl5 scl21 pat1* mutant following ablation of an epidermal or cortical cell, respectively (Figure 3D).

DOF3.4 operates downstream of the PAT1-branch GRAS-domain transcription factors

To explore the underlying mechanism of the root regeneration defect of the *scl5 scl21 pat1* triple mutant, an RNA-seq experiment was performed, comparing the transcriptome of 2-mm root tips, both under control conditions and following a 24-h bleomycin treatment, using Col-0 plants as control. When comparing Col-0 and the *scl5 scl21 pat1* triple mutant grown under the untreated condition, no significant differential gene expression was observed (FDR 0.05), except for the three targeted genes, *SCL5*, *SCL21* and *PAT1*, underscoring the absence of any phenotype under control conditions. Under the bleomycin-treated condition, 1,461 genes in Col-0 and 1,746 genes in s*cl5 scl21 pat1* were differentially expressed compared with their respective mocks (Supplemental Data Sets S2-S3). To pinpoint the genes responsible for the impaired root regeneration phenotype of the *scl5 scl21 pat1* mutant, we divided these genes into three classes. The first class of genes were those that were upregulated in both genotypes upon bleomycin treatment (Supplemental Data Set S4). The second class holds genes only upregulated in Col-0 following bleomycin treatment (Supplemental Data Set S5), whereas the third group includes genes only upregulated in the *scl5 scl21 pat1* triple mutant (Supplemental

Data Set S6). Using this subgrouping, in total 1,022 genes were found, among which 468 genes were upregulated in both genotypes, 317 specifically in Col-0, and 237 specifically in *scl5 scl21 pat1*. In the resulting gene list, the *DNA-BINDING ONE FINGER 3.4* (*DOF3.4*) transcription factor gene was identified as one of the genes showing a high fold-induction in Col-0 following bleomycin treatment, but not in the *scl5 scl21 pat1* triple mutant (Table 2). *DOF3.4* belongs to a gene family of which members have been characterized in the context of periclinal cell division during vascular development (Miyashima et al., 2019; Smet et al., 2019). Seeing the need for periclinal cell divisions in the recovery process of bleomycin-treated root tips (Heyman et al., 2016; Canher et al., 2020), the *DOF3.4* gene appeared as a good candidate gene for driving cell divisions in the root regeneration process.

To study the putative role of DOF3.4 in the context of tissue regeneration, a *pDOF3.4:NLS-GFP/GU*S reporter line was constructed, fusing its promoter (1,642 kb) to *NLS-GFP/GUS*. Under control conditions, *DOF3.4* expression within the root meristem appeared variable. During the initial days of growth, weak expression could be seen in the entire root meristem, including columella cells (Supplemental Figure S9A), however, at later growth stages, its expression was only sporadically observed in SCN cells, including cell initials of cortex/endodermis (Supplemental Figure S9B). *DOF3.4* expression mostly appeared in paired neighboring cells, suggesting a correlation between expression and recent cell division. Following treatment with bleomycin for 24 h, its expression was strongly induced in the SCN and columella cells, confirming the RNA-seq data (Figure 4A). To confirm dependence of its expression on the GRAS transcription factors, the *pDOF3.4:NLS-GFP/GU*S reporter line was introduced in the *scl5 scl21 pat1* triple mutant background, showing that the *DOF3.4* expression pattern appeared variable as well (Figure 4B), being largely identical to that observed in the wild-type background under non-wounded conditions. However, upon stem cell death following bleomycin application, *DOF3.4* expression was strongly reduced in the *scl5 scl21 pat1* triple mutant and remained notably weaker compared with the wild type during the 24, 48 and 72 h recovery time points (Figure 4B). Seeing the observed regeneration defects of the *scl5 scl21 pat1* triple mutant following root tip excision, we also mapped *DOF3.4* expression in this regeneration setup. In wild-type plants, *DOF3.4* expression was strongly activated in endodermis and cortex cell layers of the remaining stump after tip removal and subsequently expanded to inner cell layers during root tip re-establishment (Figure 4C).

Since the GRAS proteins interact with ERF115 and the triple GRAS mutant shows a regeneration phenotype resembling that of the dominant-negative version of *ERF115*, we tested whether *DOF3.4* expression was affected in the dominant-negative *ERF115*^{SRDX} background

by introgression of the *pDOF3.4:NLS-GFP/GUS* reporter construct. The resulting F1 seedlings were treated with bleomycin and recovery was followed on a bleomycin-free medium. In contrast to the strong transcriptional activation observed in wild-type plants, *DOF3.4* expression was strongly attenuated in *ERF115*^{SRDX} root tips (Figure 5A), reminiscent of the response observed for the *scl5 scl21 pat1* triple mutant (Figure 4D). This observation was confirmed through quantitative reverse-transcription PCR (RT-qPCR, Figure 5B), suggesting direct control of *DOF3.4* promoter activity by ERF115. Concordantly, previously published data generated from a tandem chromatin affinity purification experiment using ERF115 as bait, followed by sequencing, revealed an enrichment of *DOF3.4* promoter sequences (Supplemental Figure S10; Heyman et al., 2013).

DOF3.4 drives periclinal divisions in the cortex and epidermal layer

A *dof3.4* T-DNA insertion mutant showed only a mild phenotype upon bleomycin recovery, where only 20% of the seedlings showed an impaired stem cell recovery, compared with 13% in the wild-type plants (Supplemental Figure S11A), probably due to gene redundancy in the large DOF-type transcription factor family (Zhang et al., 2022). Regeneration after root tip excision also did not show any significant differences between both genotypes (Supplemental Figure S11B). Therefore, to gain functional insight into the role of *DOF3.4*, we adopted a chimeric repressor silencing technology to convert *DOF3.4* into a dominant-negative regulator by fusing it with the EAR-motif repression domain. Two independent *DOF3.4*^{SRDX} expression lines were generated (Supplemental Figure S11D), which displayed a statistically significant reduction in root tip regeneration following excision (Supplemental Figure S11E), despite the lack of an obvious root length or meristem phenotype (Supplemental Figure S11, C and F).

To assess the possibility of DOF3.4 driving the regeneration process through activation of cell divisions, we made use of *DOF3.4* overexpression lines. Within independent segregating T2 populations, we observed a Mendelian inheritance (1:1:2) of wild-type plants with a long root phenotype, homozygous (Hmz) plants with a short root and hemizygous (Htz) plants with an intermediate phenotype (Figure 6A), suggesting a dose-dependent effect of DOF3;4 on root growth. The Hmz *DOF3.4*^{OE} plants were marked by a thick root diameter (Figure 6B). To investigate in detail the root phenotype of these overexpression lines, radial sections of *DOF3.4*^{OE} roots were examined. A significant increase in the epidermis and vascular cell numbers was observed in both the Hmz and Htz *DOF3.4*^{OE} lines; those in the cortex and endodermis were only significantly increased in Hmz plants, although an increase was also observed in the endodermis cell number in Htz plants (Figure 6, C and D). Division plane

orientations indicated that the increase in cell number was in part due to periclinal divisions in the endodermal, cortical and epidermal cell layers (Figure 6C).

Since constitutive overexpression of *DOF3.4* resulted in a severe growth phenotype, inducible lines were generated by fusing the transcription factor to the glucocorticoid receptor (GR) domain. Following 24 h of dexamethasone (DEX) treatment, confocal imaging of root sections revealed a statistical increase in the number of epidermal, cortical, endodermal and vascular cells in *DOF3.4*^{GR} roots compared with mock-treated roots (Supplemental Figure S12), reminiscent of *DOF3.4*^{OE} seedlings (Figure 6D). When grown for 55 h on DEX-supplemented medium, these *DOF3.4*^{GR} inducible lines phenocopied (Figure 7A) the drastic root radial expansion trait of the constitutive *DOF3.4*^{OE} Hmz plants (Figure 6B). This root thickening was accompanied by an increase in stem cell activity, as exemplified by an increased number of columella stem cell layers, as visualized by pseudo-Schiff staining (Figure 7B). A similar increase in columella stem cell layers has been observed upon increased activity of the D-type cyclin *CYCD3;3* (Forzani et al., 2014), matching the previously reported observation that DOF3.4 acts as a transcriptional activator of the *CYCD3;3* gene (Skirycz et al., 2008). Therefore, we analyzed the expression of *CYCD3;3* in the *DOF3.4*^{GR} lines, revealing an expansion of the *CYCD3;3* expression domain from the distal columella to the columella stem cells already after 24 h and further increasing after 48 h of DEX treatment (Figure 7C).

We further reasoned that DOF3.4-targeted D-type cyclins might be involved in the regeneration process following root tip removal. Interestingly, already the single *cycd3;3* mutant showed a significant reduction in the root tip regeneration after excision (Figure 7D). This defect was enhanced in the *cycd3* triple mutant (*cycd3;1 cycd3;2 cycd3;3*) that showed a drastic reduction in regeneration 72 h post root tip excision. These data suggest a putative role of D-type cyclins during the root regeneration process.

Discussion

PAT1-branch transcription factors are required for wound regeneration

The ERF115 transcription factor is indispensable for the regeneration of a damaged root meristem (Heyman et al., 2013), with its cell division capacity being dramatically enhanced through heterodimerization with PAT1 (Heyman et al., 2016). Reversely, although both *erf115* and *pat1* mutants display a regeneration defect following root tip excision, this phenotype is not as penetrant as that of the dominant-negative *ERF115*^{SRDX} line, suggesting gene redundancy at the level of both ERF115 and PAT1. Here, through Y2H and protein affinity purification experiments, we illustrated that both ERF114 and ERF115 display redundancy in their

interaction with different members of the PAT1-branch of GRAS transcription factors. Moreover, we demonstrated that the combined activity of at least SCL5, SCL21 and PAT1 to be an absolute requirement for regeneration following wounding. Additionally, their ectopic coexpression with either *ERF114* or *ERF115* resulted in hyperproliferation phenotypes that were distinct depending on the combinations, with phenotypes for heterodimers with ERF115 being more outspoken than those with ERF114. Likewise, combinations with SCL21 yielded a more outspoken hypocotyl-derived callus phenotype, compared with combinations with SCL5 or PAT1. Although it cannot be ruled out that these distinct phenotypes originate from differences in ectopic expression levels or protein stability, a part of it might be attributed to the recognition of different target genes. It has been reported before that the related *PSK2* and *PSK5* genes are both a target of ERF115, but only the latter is controlled by ERF114 (Kong et al., 2018). Additionally, we have previously reported a tissue-specific expression of *ERF114* and *ERF115*, with both showing a similar response following wounding, but with *ERF114* and *ERF115* being expressed in the lateral root founder cells and underlying maturing protoxylem cells, respectively (Canher et al., 2022), suggesting some subfunctionalization between different ERF-GRAS heterodimers.

Among the GRAS-domain transcription factors, Arabidopsis HAM proteins are important for the maintenance of indeterminate growth (Engstrom, 2012; Geng and Zhou, 2021), whereas SHR and SCR are indispensable for the specification of the root SCN as well as the radial patterning of the root (Helariutta et al., 2000; Nakajima et al., 2001), with the corresponding mutants displaying outspoken developmental phenotypes. Differently, the *scl5 scl21 pat1* triple mutant appeared identical to the wild-type plants under unwounded control conditions in every examined aspect, being supported by the lack of any differential gene expression between wild-type and mutant plants under control conditions, at least within the root meristem. Contrary, the triple mutant plants were hypersensitive to bleomycin that triggers vascular cell death, resulting in a collapse of the root meristem. This phenotype is most likely due to a regeneration defect rather than an impaired DNA damage response, as both genotypes share a similar transcriptional activation of genes involved in DNA double-strand break repair, oxidative stress, and DNA biosynthesis following bleomycin treatment. Moreover, a similar regeneration failure was observed following root tip excision, as well as a reduced potential to induce periclinal divisions following laser-mediated single cell ablation. Interestingly, the list of genes being specifically upregulated in the *scl5 scl21 pat1* mutant background following bleomycin treatment relates to cell wall organization and biogenesis (Supplemental Data Set S7). Such enrichment likely reflects the loss of division competence following wounding,

resulting in cell enlargement rather than cell division. These data thus suggest the specific involvement of these three GRAS-domain proteins in maintaining stem cell activity following wounding, although it is still possible that contributions to normal developmental processes in the absence of wounding are masked by the remaining other two members of the PAT1 subfamily, being *SCL1* and *SCL13*.

DOF3.4 activates periclinal cell division upon wounding

RNA-sequencing identified the DOF3.4 transcription factor as a novel molecular component controlling regeneration in an SCL5/SCL21/PAT-dependent manner. Under control conditions, *DOF3.4* transcription is hardly detectable in the young root meristem, most frequently occurring in paired cells, indicative of expression correlating with stem cell division. Although a uniform *pDOF3.4:NLS-GFP* expression pattern could be detected in 2-day-old root meristems, expression dramatically declined in the 5-day-old root, suggestion the that early expression pattern represents an remnant of expression during embryogenesis. Indeed, *DOF3.4* is strongly expressed in the embryo proper and suspensor cells (Skirycz et al., 2008; Babu et al., 2013). Therefore, under control conditions, DOF3.4 activity might be restricted to early embryonic development. In contrast, upon wounding we observed a strong transcriptional activation of *DOF3.4*. Calling upon the embryonic role of DOF3.4 during regeneration supports the model put forward based on single-cell transcriptome analysis, demonstrating that stem cell reformation following root tip excision is preceded by rapid cell identity transitions and developmental events that closely resemble that of embryonic root formation (Efroni et al., 2016).

Differently from the *DOF3.4*^{SRDX} line, no clear developmental or regeneration-related phenotypes could be observed for an available T-DNA insertion line, suggesting putative redundancy with other DOF transcription factors. Accordingly, DOF family members have been linked with proliferation and regeneration before, with *DOF5.4* promoting callus formation (Ramirez-Parra et al., 2017), whereas *HIGH CAMBIAL ACTIVITY2* controls grafting dynamics, likely by promoting cell division and cambium formation to enhance wound healing (Konishi and Yanagisawa, 2007; Guo et al., 2009; Gardiner et al., 2010; Melnyk et al., 2018). The latter has recently been demonstrated to operate redundantly with the related TMO6 and DOF2.1 transcription factors, whereas *DOF3.4* expression was found as well to be rapidly and strongly induced following grafting (Zhang et al., 2022). We therefore speculate that the DOF3.4^{SRDX} protein targets other DOF transcription factors that might work together with

DOF3.4, although no such other *DOF* gene was found to be significant differentially expressed in control versus *scl5 scl21 pat1* mutant plants following bleomycin treatment.

DOF3.4 holds the potential to drive periclinal cell divisions, as illustrated by the cell division phenotypes in the vascular bundle, ground tissues and epidermis following its overexpression. This potential is shared with different DOF factors that have been demonstrated to redundantly control periclinal cell divisions in vascular tissues (Papi et al., 2002; Ward et al., 2005; Fornara et al., 2009; Rueda-Romero et al., 2012; Miyashima et al., 2019; Smet et al., 2019). However, differently from these *DOF* genes, we failed to detect within seedlings any *DOF3.4* expression in the vascular cells under unstressed conditions. It indicates that DOF3.4's function post embryogenesis might be restricted to regeneration.

Previously, the *CYCD3;3* gene was demonstrated to be a direct DOF3;4 target (Skirycz et al., 2008). Accordingly, excised *cycd3;3* root tips displayed a regeneration phenotype, being aggravated in the *cycd3;1 cycd3;2 cycd3;3* triple mutant. Likewise, the mutant is less efficient in wound-induced callus formation following a hypocotyl cut, compared to wild type plants (Ikeuchi et al., 2017). These data suggest that D3-type cyclins might be among the most important targets of DOF3.4 in the regeneration process. In wild-type plants, *CYCD3;3* expression can be found in the vascular initials and most distal columella cells. The latter might again be a remnant of *CYCD3;3* requirement for division activity during establishment of the embryonic columella (Forzani et al., 2014). Upon inducible *DOF3.4*^{GR} expression, the *CYCD3;3* expression domain expanded to the columella stem cells within 48 h of DEX induction, cells in which *DOF3.4* expression could be also observed following bleomycin treatment. Thus, activation of *CYCD3;3* by DOF3.4 might explain the extra layers of columella stem cells observed in the *DOF3.4*^{GR} lines. An enhanced stem cell division rate is a feature shared with RBR1-deficient plants (Wildwater et al., 2005; Wachsman et al., 2011; Weimer et al., 2012; Cruz-Ramírez et al., 2013), indicating that DOF3.4 might operate through inactivation of RBR1, facilitated by phosphorylation by D-type cyclin CDK complexes (Nakagami et al., 1999). Seeing the phenotypic resemblance with RBR1 RNAi lines, it is likely that DOF3.4 converges on the RBR1 pathway through the transcriptional activation of *CYCD3;3* (Wildwater et al., 2005). Another interesting feature of CYCD3s is that they act downstream of cytokinin signaling (Dewitte et al., 2007). Correspondingly, endogenous cytokinin levels have been found to rise after wounding of etiolated hypocotyls (Ikeuchi et al., 2017), but whether the DOF3.4 activated *CYCD3* response following wounding in the root meristem is achieved through the cytokinin pathway rather than being downstream of a transcriptional cascade instigated by ERF115, still needs to be demonstrated.

In addition to *DOF3.4*, the auxin-responsive *INDOLE-3-ACETIC ACID INDUCIBLE 5* (*IAA5*) gene was found among the strongest SCL5/SLC21/PAT1-responsive genes. Accordingly, *IAA5* expression is wound responsive (Asahina et al., 2011; Matsuoka et al., 2016; Ikeuchi et al., 2017). IAA is a canonical AUX/IAA protein that inhibits distal stem cell differentiation by repressing the transcriptional auxin response (Lv et al., 2020), indicative for a role in acquiring or maintaining stem cell regeneration during the regeneration process. However, further experiments are needed to verify this claim.

ERF-GRAS heterodimerization driving cell divisions via DOF3.4

Next to a strong reduction in the transcriptional activation of *DOF3.4* following bleomycin treatment of the *scl5 scl21 pat1* triple mutants, its expression was strongly repressed in the *ERF115*^{SRDX} background. These data suggest that it is most likely a dimer between ERF115 and the PAT1-type GRAS-domain transcription factors that controls *DOF3.4* expression. However, the relative contribution of both subunits in its transcriptional activation still needs to be clarified. Whereas ERF proteins directly bind to DNA using their AP2 domain (Ohme-Takagi and Shinshi, 1995), GRAS-domain proteins have been suggested to be transcriptional cofactors that interact with other transcription factors (Hirano et al., 2017) or histone deacetylases (Gao et al., 2004; Gao et al., 2015) to indirectly bind to DNA. Accordingly, we failed to detect a direct binding of GRAS proteins to the *DOF3.4* promoter. Contrary, previously published tandem chromatin affinity purification data revealed a putative binding site for ERF115 on the *DOF3.4* promoter region (Supplementary Figure S10) (Heyman et al., 2013). It is therefore tempting to speculate that the ERF transcription factor provides target gene specificity, whereas the GRAS interaction partner controls the regulation of its transcription by recruiting histone-modifying enzymes. However, indirect control of expression by ERF115 cannot be excluded, since *DOF3.4* has been recently described as an auxin-induced gene being under putative transcriptional control of MP/ARF5 (Larrieu et al., 2022). At the other hand, *MP/ARF5* was reported to be a *bona fide* direct ERF115 target gene (Canher et al., 2020), in that way still placing *DOF3.4* downstream of the wound-induced ERF115-dependent transcriptional pathway.

Taken together, our data pinpoint DOF3.4 as a novel and important target operating downstream of at least ERF115 in complex with SCL5, SCL21, or PAT1. Whereas the previously identified targets *PSK2/PSK5*, *WIND1* and *MP/ARF5* play a role in promoting cell proliferation, cellular reprograming and inducting stem cell fate, respectively, DOF3.4 appears to play an important role in driving periclinal divisions needed for tissue repair through

transcriptional induction of D3-type cyclins (Figure 8). Additionally, our work suggests the presence of a multitude of putative ERF-GRAS heterodimeric combinations that may play different roles in initiating the regeneration program, probably underscoring the plasticity of tissue recovery following damage.

Materials and methods

Plant medium and growth conditions

Arabidopsis seeds were sterilized in 70% ethanol for 10-15 min and subsequently washed with 100% ethanol, after which they were left to dry in sterile conditions. For all experiments, the seeds were stratified in the dark for 2 days at 4°C before being placed in the growth room. Plants were grown *in vitro* under long-day conditions (16-h light/8-h dark, Lumilux Cool White lm, 50 to 70 µmol m^{-2} s^{-1}) at 21°C on solidified half-strength Murashige and Skoog (MS) medium (2.151 g/L, 10 g/L sucrose, and 0.5 g/L 2-(N-morpholino) ethanesulfonic acid (MES), adjusted to pH 5.7 with 1 M KOH and 8 or 10 g/L plant agar). Dexamethasone (DEX; Sigma) treatments were performed by either germinating seeds on 10 µM DEX-supplemented medium or by transferring plants from ½ MS to 10 µM DEX-supplemented medium.

Constructs and lines

In all experiments, the Col-0 ecotype was used. Primers used for cloning and genotyping can be found in Supplemental Table S1. *ERF114*^{OE}, *ERF115*^{OE}, *PAT1*^{OE}, *ERF115*^{SRDX}, *pat1*, *erf115*, *pWOX5:NLS-GFP/GUS*, *pERF115:NLS-TdTomato* and *pERF114:NLS-GFP/GUS* have been described previously (Heyman et al., 2016; Canher et al., 2022). The *scl21* (SALK_146085), *scl5* (SALK_152973) and *dof3.4* (SALK_049540) mutants were obtained from the Salk Institute T-DNA Express database (Alonso et al., 2003). The *cycd3;3* single and *cycd3;1 cycd3;2 cycd3;3* triple mutants were described previously (Dewitte et al., 2007). *DOF3.4*^{OE}, *SCL5*^{OE}, and *SCL21*^{OE} constructs were generated by cloning their wild-type ORF including the stop codon into pDONR221 (Invitrogen) via a BP reaction and subsequently recombining it via an LR reaction behind the strong *Cauliflower Mosaic Virus* (*CaMV*) *35S* promoter in the pB7WG2 vector for *DOF3.4* and *SCL5* and the pH7WG2 vector for *SCL21* (Karimi et al., 2002). For GFP reporter constructs, the promoter region immediately upstream of the start codon of *DOF3.4* (1,642 bp), and *SCL5* (2,525 bp), was inserted into the pMK7S*NFm14GW plasmid (Karimi et al., 2002). Translational reporter *pSCL5:SCL5-GFP* and *pPAT1:PAT1-GFP* lines were obtained by cloning each genomic fragment, 4,626 bp and 5,267 bp respectively, containing the promoter and coding region without stop in pDONRP4P1r, followed by fusion

of the GFP reporter without NLS to the C-terminus of each coding sequence and finally, combined in the destination vectors pHm42GW and pBm42GW, respectively. The *pCYCD3;3:GFP/GUS* reporter line was generated through Gateway cloning of the 2,199 bp preceding the translation initiation codon sequence into pKGWFS7 as described previously (Benhamed et al., 2008). The *pDOF3.4:NLS-GFP/GUS* reporter was introduced in the *ERF115*^{SRDX} background via crossing.

GRAS triple mutants harboring the *pDOF3.4:NLS-GFP/GUS* reporter were generated by transformation of the pFASTRK-II-m43GW destination vector carrying the *DOF3.4* promoter, upstream of the *NLS-GFP* and *GUS* reporter sequences, in the *scl5 scl21 pat1* triple mutant. Similarly, the *pWOX5:NLS-GFP/GUS* reporter construct (Heyman et al., 2016) was introduced in the GRAS triple mutant by floral dip-mediated transformation and transformants were selected based on the presence of *WOX5-GFP* derived fluorescence. *DOF3.4*^{GR} was generated by recombining the *DOF3.4* coding sequence without stop before the *GLUCOCORTICOID RECEPTOR* coding sequence under control of the *CaMV 35S* promoter in the pFASTHm43GW destination vector.

The *DOF3.4*^{SRDX} construct was generated by fusing the *DOF3.4* coding region without stop codon with the SRDX domain (LDLDLELRLGFA) and recombined into the pH7GW2 expression vector under the control of the *CaMV 35S* promoter via Gateway recombination.

All constructs were transferred into the *Agrobacterium tumefaciens* C58C1RifR strain harboring the pMP90 plasmid. The obtained Agrobacterium strains were used to generate stably transformed Arabidopsis lines with the floral dip transformation method (Clough and Bent, 1998). Higher order mutants were generated by crossing.

Yeast two-hybrid assay

Yeast constructs were generated by recombining the respective ERF and GRAS cDNA clones into the pDEST32 and pDEST22 plasmids using Gateway recombination, generating the bait and prey clones, respectively. Primer sequences used for cDNA clone and N-terminal ERF fragment isolation can be found in Supplemental Table S1 or have been described previously (Heyman et al., 2016). Plasmids encoding the bait and prey were transformed into the yeast strain PJ69-4α (MATα; trp1-901, leu2-3,112, ura3-52, his3-200, gal4Δ, gal80Δ, LYS2::GAL1-HIS3, GAL2-ADE2, met2GAL7-lacZ) and PJ69-4a (MATa; trp1-901, leu2-3,112, ura3-52, his3-200, gal4Δ, gal80Δ, LYS2TGAL1-HIS3, GAL2-ADE2, met2TGAL7-lacZ) by the LiAc method (Gietz et al., 1992). For the interaction test between the newly annotated *SCL5* and the *ERF A*-fragments, the respective pDEST22 and pDEST32 plasmids were cotransformed in the

PJ69-4a strain. Transformed yeast cells were selected on synthetic dextrose plates without Leu (pDEST 32) or without Trp (pDEST22). Interactions between proteins were assayed by the mating method. All pDEST32 yeast cultures were inoculated in 200 µL synthetic dextrose without Trp in a 96-well microtiter plate (Falcon; BD Biosciences), whereas one pDEST22 yeast culture was inoculated in 50 mL synthetic dextrose medium without Leu. To scale up the yeast cultures, 20 µL of each culture grown for 2 d at 30°C was added to a microtiter plate containing 125 µL of Glc-containing rich medium (10 g/L bacto-yeast extract, 10 g/L bacto-peptone, and 20% dextrose) and again grown for 24 h at 30°C. The Glc-containing rich medium was replaced by synthetic dextrose medium without Leu and Trp. Diploid strains grown in a 96-well microtiter plate (NUNC) for 2 d at 30°C were diluted 1/10 prior to spotting on agar-solidified synthetic dextrose medium without Leu and Trp but with His (as control), or synthetic dextrose medium without Leu, Trp, or His, in the presence of 3AT. Growth was observed after 3 d of incubation at 30°C.

Root sectioning

For Technovit sectioning, 6-day-old seedlings were fixed in a paraformaldehyde (4%)-gluteraldehyde (1%) solution, dehydrated through a graded ethanol series and embedded in Technovit 7100 (Heraeus Kulzer). Sections of 4-µm thickness were prepared and counterstained as described in De Smet et al. (2004).

Confocal and light microscopy

Arabidopsis roots were stained using propidium iodide (PI) by incubation in a 10-µM solution for 2 min before imaging. For confocal microscopy, a Zeiss LSM5 and LSM710 confocal microscope were used. GFP fluorescence was observed after excitation using a 488-nm laser. PI fluorescence was observed after excitation using a 543-nm laser. GFP and tdTomato emissions were collected at 500-530nm and 570-630nm, respectively. For light and differential interference contrast microscopy, an Olympus BX51 microscope was used. Pseudo-Schiff PI staining was performed as described (Canher et al., 2020).

Recovery experiments

For bleomycin treatment, 5-day-old seedlings were transferred to vertical plates supplemented with 0.6 µg/mL bleomycin. For recovery, seedlings were retransferred to control medium after 24 h of growth on bleomycin-containing medium and allowed to recover for five days. For the bleomycin recovery percentage, unless stated otherwise, plant recovered for five days from the

bleomycin treatment were imaged under the confocal microscope and scored for regenerated versus non-regenerated based on meristem organization, after staining the roots with PI solution. Root tip excisions were performed as described previously (Sena et al., 2009). Root tip regeneration 72 h after removal was scored negative when a collapse of the root meristem was observed. For laser ablation, an LSM710 confocal microscope with a 405-nm laser was used at 70% laser power for 5-10 s. For periclinal division quantification, epidermal and cortical cells were ablated and periclinal divisions were assessed in the cortex and endodermis, respectively, 16 h post ablation. The percentage of periclinal divisions was scored as previously described (Marhava et al., 2019).

RT-qPCR

RNA was isolated from the seedlings with the RNeasy Plant Mini kit (Qiagen). DNase treatment was done with the RQ1 RNase-Free DNase (Promega) prior to cDNA synthesis with the iScript cDNA Synthesis kit (Bio-Rad). Relative expression levels were determined by RT-qPCR with the LightCycler 480 Real-Time SYBR Green PCR System (Roche). *EMB2386* and *PAC1* were used as reference genes for normalization. Primer sequences used for RT-qPCR are listed in Supplemental Table S1.

RNA-seq experiment

Five days after germination, seedlings were transferred on mesh to either fresh control medium or medium supplemented with 0.9 μg/mL bleomycin for 24 h. Root tips (approximately 2 mm) were collected in liquid nitrogen in three biological repeats. At least 100 roots were used per biological repeat. RNA from samples was extracted using the RNeasy Plant Mini kit (QIAGEN) according to the manufacturer's protocols. A total amount of 1 μg RNA per sample was used as input material for the RNA sample preparations. Sequencing libraries were generated using NEBNext® UltraTM RNALibrary Prep Kit for Illumina® (NEB, USA) following manufacturer's recommendations and index codes were added to attribute sequences to each sample. Samples were sequenced on an Illumina NovaSeq6000 instrument and 150-bp paired-end reads were generated. Transcript quantification was performed by Salmon version 0.9.1 (Patro et al., 2017), using the Araport11 list of all coding sequences (Cheng et al., 2017). The option to correct for a sequence-specific bias was turned off and all parameters were set to their default values. Transcript quantification results generated by Salmon were corrected for gene length variations across the samples using the tximport 1.6.0 R package (Soneson et al., 2015) and were further analyzed using the edgeR package (Robinson et al., 2010). Transcripts with a

read count of less than 10 in all samples combined were removed from further analyses. Normalized read counts were log2 transformed, and a quasi-likelihood negative binomial generalized linear model was fitted to the data using genotype, treatment and the genotype x treatment interaction term as factors to identify differential gene expression.

Single-step immunoprecipitation and mass spectrometry

Three pull-down experiments on Arabidopsis cell suspension cultures expressing N-terminally GS^{TEV}-tagged ERF115 were performed as described (Van Leene et al., 2019). On-bead digested samples were analyzed on a Q Exactive HF (ThermoFisher Scientific) and co-purified proteins were identified using standard procedures (Van Leene et al., 2015). After identification, the obtained protein list was filtered versus a list of non-specific proteins, assembled similarly as described (Van Leene et al., 2015). True interactors that might have been filtered out because of their presence in the list of non-specific proteins were retained by means of quantitative analysis using the average normalized spectral abundance factors (NSAF) of the identified proteins in the ERF115 pull-downs. Proteins identified with at least two peptides in at least two experiments, showing high (at least tenfold) and significant [$-\log_{10}$(p-value(T-test)) ≥ 10] enrichment compared with calculated average NSAF values from a large data set of pull-downs with non-related bait proteins, were retained.

Bimolecular fluorescence complementation

The newly annotated *SCL5* ORF was tagged at the carboxy-terminal end with the GFP tail fragment and inserted into the pK7m34GW vector under control of the *CaMV 35S* constitutive promoter using Gateway cloning. The *ERF115* and *SCL21* constructs were described previously (Heyman et al., 2016). For *Nicotiana benthamiana* leaf blade infiltration, equal concentrations (final $A_{600} = 0.5$) of a 2-day-old liquid grown *Agrobacterium tumefaciens* culture containing the respective constructs were incubated in infiltration buffer (10 mM $MgCl_2$, 10 mM MES (pH 5.6), 0.1 mM acetosyringone) for 2 h before infiltration of 6-week-old plants. Plants were allowed to grow for another 2 days before observing the interaction by means of confocal microscopy. As a negative control, single constructs were infiltrated, yielding no detectable GFP signal.

Statistical analysis

Statistical analyses were performed as indicated in the figure legends.

Accession numbers

RNA-seq raw data from this study were deposited in Gene Expression Omnibus (accession number: GSE200500). Sequence data from this article can be found in the Arabidopsis Genome Initiative or GenBank/EMBL databases under the following accession numbers: *ERF114* (*At5g61890*); *ERF115* (*At5g07310*); *PAT1* (*At5g48150*); *SCL5* (*At1g50600*); *SCL21* (*At2g04890*); *DOF3.4* (*At3g50410*); *CYCD3;3* (*At5g50050*).

Supplemental data

The following materials are available in the online version of this article.

Supplemental Figure S1. Corrected annotation of the *SCL5* promoter and coding sequence.

Supplemental Figure S2. Bimolecular fluorescence complementation between ERF115 and SCL5.

Supplemental Figure S3. Fluorescence intensity overlap between the *ERF115* and *SCL5* transcriptional reporters following bleomycin treatment.

Supplemental Figure S4. Root length of 12-day-old Col-0, *ERF114*, *ERF115*, *SCL5*, *SCL21* and *PAT1* single and *ERF114-SCL5*, *ERF114-SCL21*, *ERF114-PAT1 ERF115-SCL5*, *ERF115-SCL21* and *ERF115-PAT1* co-overexpressing seedlings

Supplemental Figure S5. Root length of *ERF115*, *PAT1*, *SCL5*, *SCL21* and respective co-overexpressing lines.

Supplemental Figure S6. Growth phenotypes of *ERF114*, *PAT1*, *SCL5*, *SCL21* and respective co-overexpressing lines.

Supplemental Figure S7. Rosettes of 25-day-old Col-0, *ERF114*, *ERF115*, *SCL5*, *SCL21*, *PAT1* overexpressing lines and their respective combinations.

Supplemental Figure S8. *GRAS* higher order mutants do not show a meristem phenotype under control conditions.

Supplemental Figure S9. *DOF3.4* expression in root meristem.

Supplemental Figure S10. DNA binding of ERF115 to the *DOF3.4* promoter.

Supplemental Figure S11. *DOF3.4*^{SRDX} seedlings display a reduced regeneration efficiency following root tip excision.

Supplemental Figure S12. Activation of *DOF3.4*^{GR} activates periclinal cell divisions.

Supplemental Table S1. Primer sequences.

Supplemental Data Set S1. Protein Identification details obtained with the Q Exactive HF (Thermo Fisher Scientific) and Mascot Distiller software (version 2.5.0.0, Matrix Science)

combined with the Mascot search engine (version 2.5.1, Matrix Science) using the Mascot Daemon interface and database TAIRplus (Van Leene et al., 2015).

Supplemental Data Set S2. List of genes being differentially expressed (FDR < 0.05) in wild-type root tips (2 mm) following bleomycin treatment.

Supplemental Data Set S3. List of genes being differentially expressed (FDR < 0.05) in *scl5 scl21 pat1* root tips (2 mm) following bleomycin treatment.

Supplemental Data Set S4. List of genes being differentially activated (FDR < 0.05) in both wild-type and *scl5 scl21 pat1* root tips (2 mm) following bleomycin treatment.

Supplemental Data Set S5. List of genes being differentially activated (FDR < 0.05) in wild-type root tips only following bleomycin treatment.

Supplemental Data Set S6. List of genes being differentially activated (FDR < 0.05) in *scl5 scl21 pat1* root tips only following bleomycin treatment.

Supplemental Data Set S7. GO enrichment of the list of genes being activated following bleomycin treatment in *scl5 scl21 pat1* root tips only.

Acknowledgments

The authors thank Annick Bleys for critically reading of the manuscript. This work was supported by grants of the Research Foundation Flanders (G007218N and G010820N). Ran Lu was supported by the China Scholarship Council (201704910848).

References

Aida, M., Beis, D., Heidstra, R., Willemsen, V., Blilou, I., Galinha, C., Nussaume, L., Noh, Y.-S., Amasino, R., and Scheres, B. (2004). The *PLETHORA* genes mediate patterning of the *Arabidopsis* root stem cell niche. Cell **119,** 109-120.

Alonso, J.M., Stepanova, A.N., Leisse, T.J., Kim, C.J., Chen, H., Shinn, P., Stevenson, D.K., Zimmerman, J., Barajas, P., Cheuk, R., Gadrinab, C., Heller, C., Jeske, A., Koesema, E., Meyers, C.C., Parker, H., Prednis, L., Ansari, Y., Choy, N., Deen, H., Geralt, M., Hazari, N., Hom, E., Karnes, M., Mulholland, C., Ndubaku, R., Schmidt, I., Guzman, P., Aguilar-Henonin, L., Schmid, M., Weigel, D., Carter, D.E., Marchand, T., Risseeuw, E., Brogden, D., Zeko, A., Crosby, W.L., Berry, C.C., and Ecker, J.R. (2003). Genome-wide insertional mutagenesis of *Arabidopsis thaliana*. Science **301,** 653-657.

Asahina, M., Azuma, K., Pitaksaringkarn, W., Yamazaki, T., Mitsuda, N., Ohme-Takagi, M., Yamaguchi, S., Kamiya, Y., Okada, K., Nishimura, T., Koshiba, T., Yokota, T., Kamada, H., and Satoh, S. (2011). Spatially selective hormonal control of RAP2.6L and ANAC071 transcription factors involved in tissue reunion in *Arabidopsis*. Proc. Natl. Acad. Sci. USA **108,** 16128-16132.

Babu, Y., Musielak, T., Henschen, A., and Bayer, M. (2013). Suspensor length determines developmental progression of the embryo in Arabidopsis. Plant Physiol. **162,** 1448-1458.

Benhamed, M., Martin-Magniette, M.-L., Taconnat, L., Bitton, F., Servet, C., De Clercq, R., De Meyer, B., Buysschaert, C., Rombauts, S., Villarroel, R., Aubourg, S., Beynon, J., Bhalerao, R.P., Coupland, G., Gruissem, W., Menke, F.L.H., Weisshaar, B., Renou, J.-P., Zhou, D.-X., and Hilson, P. (2008). Genome-scale Arabidopsis promoter array identifies targets of the histone acetyltransferase GCN5. Plant J. **56,** 493-504.

Bolle, C. (2004). The role of GRAS proteins in plant signal transduction and development. Planta **218,** 683-692.

Canher, B., Lanssens, F., Zhang, A., Bisht, A., Mazumdar, S., Heyman, J., Wolf, S., Melnyk, C.W., and De Veylder, L. (2022). The regeneration factors ERF114 and ERF115 regulate auxin-mediated lateral root development in response to mechanical cues. Mol. Plant **15,** 1543-1557.

Canher, B., Heyman, J., Savina, M., Devendran, A., Eekhout, T., Vercauteren, I., Prinsen, E., Matosevich, R., Xu, J., Mironova, V., and De Veylder, L. (2020). Rocks in the auxin stream: Wound-induced auxin accumulation and ERF115 expression synergistically drive stem cell regeneration. Proc. Natl. Acad. Sci. USA **117,** 16667-16677.

Cao, D., Hussain, A., Cheng, H., and Peng, J. (2005). Loss of function of four DELLA genes leads to light- and gibberellin-independent seed germination in Arabidopsis. Planta **223,** 105-113.

Cheng, C.-Y., Krishnakumar, V., Chan, A.P., Thibaud-Nissen, F., Schobel, S., and Town, C.D. (2017). Araport11: a complete reannotation of the *Arabidopsis thaliana* reference genome. Plant J. **89,** 789-804.

Cheng, H., Qin, L., Lee, S., Fu, X., Richards, D.E., Cao, D., Luo, D., Harberd, N.P., and Peng, J. (2004). Gibberellin regulates *Arabidopsis* floral development via suppression of DELLA protein function. Development **131,** 1055-1064.

Christiaens, F., Canher, B., Lanssens, F., Bisht, A., Stael, S., De Veylder, L., and Heyman, J. (2021). Pars pro toto: every single cell matters. Front. Plant Sci. **12,** 656825.

Clough, S.J., and Bent, A.F. (1998). Floral dip: a simplified method for *Agrobacterium*-mediated transformation of *Arabidopsis thaliana*. Plant J. **16,** 735-743.

Cruz-Ramírez, A., Díaz-Triviño, S., Wachsman, G., Du, Y., Arteága-Vázquez, M., Zhang, H., Benjamins, R., Blilou, I., Neef, A.B., Chandler, V., and Scheres, B. (2013). A SCARECROW-RETINOBLASTOMA protein network controls protective quiescence in the Arabidopsis root stem cell organizer. PLoS Biol. **11,** e1001724.

Curtis, M.J., and Hays, J.B. (2007). Tolerance of dividing cells to replication stress in UVB-irradiated Arabidopsis roots: requirements for DNA translesion polymerases η and ζ. DNA Repair **6,** 1341-1358.

De Smet, I., Chaerle, P., Vanneste, S., De Rycke, R., Inzé, D., and Beeckman, T. (2004). An easy and versatile embedding method for transverse sections. J. Microsc. **213,** 76-80.

Dewitte, W., Scofield, S., Alcasabas, A.A., Maughan, S.C., Menges, M., Braun, N., Collins, C., Nieuwland, J., Prinsen, E., Sundaresan, V., and Murray, J.A.H. (2007). *Arabidopsis* CYCD3 D-type cyclins link cell proliferation and endocycles and are rate-limiting for cytokinin responses. Proc. Natl. Acad. Sci. USA **104,** 14537-14542.

Duclercq, J., Sangwan-Norreel, B., Catterou, M., and Sangwan, R.S. (2011). *De novo* shoot organogenesis: from art to science. Trends Plant Sci. **16,** 597-606.

Efroni, I., Mello, A., Nawy, T., Ip, P.-L., Rahni, R., DelRose, N., Powers, A., Satija, R., and Birnbaum, K.D. (2016). Root regeneration triggers an embryo-like sequence guided by hormonal interactions. Cell **165,** 1721-1733.

Engstrom, E.M. (2012). HAM proteins promote organ indeterminacy. But how? Plant Signal. Behav. **7,** 227-234.

Fornara, F., Panigrahi, K.C.S., Gissot, L., Sauerbrunn, N., Rühl, M., Jarillo, J.A., and Coupland, G. (2009). *Arabidopsis* DOF transcription factors act redundantly to reduce *CONSTANS* expression and are essential for a photoperiodic flowering response. Dev. Cell **17,** 75-86.

Forzani, C., Aichinger, E., Sornay, E., Willemsen, V., Laux, T., Dewitte, W., and Murray, J.A.H. (2014). WOX5 suppresses *CYCLIN D* activity to establish quiescence at the center of the root stem cell niche. Curr. Biol. **24,** 1939-1944.

Fulcher, N., and Sablowski, R. (2009). Hypersensitivity to DNA damage in plant stem cell niches. Proc. Natl. Acad. Sci. USA **106,** 20984-20988.

Gao, M.-j., Parkin, I., Lydiate, D., and Hannoufa, A. (2004). An auxin-responsive SCARECROW-like transcriptional activator interacts with histone deacetylase. Plant Mol. Biol. **55,** 417-431.

Gao, M.-J., Li, X., Huang, J., Gropp, G.M., Gjetvaj, B., Lindsay, D.L., Wei, S., Coutu, C., Chen, Z., Wan, X.-C., Hannoufa, A., Lydiate, D.J., Gruber, M.Y., Chen, Z.J., and Hegedus, D.D. (2015). SCARECROW-LIKE15 interacts with HISTONE DEACETYLASE19 and is essential for repressing the seed maturation programme. Nat. Commun. **6,** 7243.

Gardiner, J., Sherr, I., and Scarpella, E. (2010). Expression of *DOF* genes identifies early stages of vascular development in *Arabidopsis* leaves. Int. J. Dev. Biol. **54,** 1389-1396.

Geng, Y., and Zhou, Y. (2021). *HAM* gene family and shoot meristem development. Front. Plant Sci. **12,** 800332.

Gietz, D., St Jean, A., Woods, R.A., and Schiestl, R.H. (1992). Improved method for high efficiency transformation of intact yeast cells. Nucleic Acids Res. **20,** 1425.

Guo, Y., Qin, G., Gu, H., and Qu, L.-J. (2009). *Dof5.6/HCA2*, a Dof transcription factor gene, regulates interfascicular cambium formation and vascular tissue development in *Arabidopsis*. Plant Cell **21,** 3518-3534.

Helariutta, Y., Fukaki, H., Wysocka-Diller, J., Nakajima, K., Jung, J., Sena, G., Hauser, M.-T., and Benfey, P.N. (2000). The *SHORT-ROOT* gene controls radial patterning of the *Arabidopsis* root through radial signaling. Cell **101,** 555-567.

Heyman, J., Canher, B., Bisht, A., Christiaens, F., and De Veylder, L. (2018). Emerging role of the plant ERF transcription factors in coordinating wound defense responses and repair. J. Cell Sci. **131,** jcs208215.

Heyman, J., Cools, T., Vandenbussche, F., Heyndrickx, K.S., Van Leene, J., Vercauteren, I., Vanderauwera, S., Vandepoele, K., De Jaeger, G., Van Der Straeten, D., and De Veylder, L. (2013). ERF115 controls root quiescent center cell division and stem cell replenishment. Science **342,** 860-863.

Heyman, J., Cools, T., Canher, B., Shavialenka, S., Traas, J., Vercauteren, I., Van den Daele, H., Persiau, G., De Jaeger, G., Sugimoto, K., and De Veylder, L. (2016). The heterodimeric transcription factor complex ERF115-PAT1 grants regeneration competence. Nat. Plants **2,** 16165.

Hirano, Y., Nakagawa, M., Suyama, T., Murase, K., Shirakawa, M., Takayama, S., Sun, T.-p., and Hakoshima, T. (2017). Structure of the SHR-SCR heterodimer bound to the BIRD/IDD transcriptional factor JKD. Nat. Plants **3,** 17010.

Hoermayer, L., Montesinos, J.C., Marhava, P., Benková, E., Yoshida, S., and Friml, J. (2020). Wounding-induced changes in cellular pressure and localized auxin signalling spatially coordinate restorative divisions in roots. Proc. Natl. Acad. Sci. USA **117,** 15322-15331.

Ikeuchi, M., Favero, D.S., Sakamoto, Y., Iwase, A., Coleman, D., Rymen, B., and Sugimoto, K. (2019). Molecular mechanisms of plant regeneration. Annu. Rev. Plant Biol. **70,** 377-406.

Ikeuchi, M., Iwase, A., Rymen, B., Lambolez, A., Kojima, M., Takebayashi, Y., Heyman, J., Watanabe, S., Seo, M., De Veylder, L., Sakakibara, H., and Sugimoto, K. (2017). Wounding triggers callus formation via dynamic hormonal and transcriptional changes. Plant Physiol. **175,** 1158-1174.

Illingworth, C.M. (1974). Trapped fingers and amputated finger tips in children. J. Pediatr. Surg. **9,** 853-858.

Iwase, A., Mitsuda, N., Koyama, T., Hiratsu, K., Kojima, M., Arai, T., Inoue, Y., Seki, M., Sakakibara, H., Sugimoto, K., and Ohme-Takagi, M. (2011). The AP2/ERF transcription factor WIND1 controls cell dedifferentiation in *Arabidopsis*. Curr. Biol. **21,** 508-514.

Karimi, M., Inzé, D., and Depicker, A. (2002). GATEWAY^{TM} vectors for *Agrobacterium*-mediated plant transformation. Trends Plant Sci. **7,** 193-195.

Kong, X., Tian, H., Yu, Q., Zhang, F., Wang, R., Gao, S., Xu, W., Liu, J., Shani, E., Fu, C., Zhou, G., Zhang, L., Zhang, X., and Ding, Z. (2018). PHB3 maintains root stem cell niche identity through ROS-responsive AP2/ERF transcription factors in *Arabidopsis*. Cell Reports **22,** 1350-1363.

Konishi, M., and Yanagisawa, S. (2007). Sequential activation of two Dof transcription factor gene promoters during vascular development in *Arabidopsis thaliana*. Plant Physiol. Biochem. **45,** 623-629.

Larrieu, A., Brunoud, G., Guerault, A., Laine, S., Hennet, L., Stigliani, A., Gildea, I., Just, J., Soubigou-Taconnat, L., Balzergue, S., Davies, B., Scarpella, E., Helariutta, Y., Parcy, F., and Vernoux, T. (2022). Transcriptional reprogramming during floral fate acquisition. iScience **25,** 104683.

Lu, R., Canher, B., Bisht, A., Heyman, J., and De Veylder, L. (2021). Three-dimensional quantitative analysis of the Arabidopsis quiescent centre. J. Exp. Bot. **72,** 6789-6800.

Lv, B., Yu, Q., Liu, J., Wen, X., Yan, Z., Hu, K., Li, H., Kong, X., Li, C., Tian, H., De Smet, I., Zhang, X.-S., and Ding, Z. (2020). Non-canonical AUX/IAA protein IAA33 competes with canonical AUX/IAA repressor IAA5 to negatively regulate auxin signaling. EMBO J. **39,** e101515.

Mähönen, A.P., ten Tusscher, K., Siligato, R., Smetana, O., Díaz-Triviño, S., Salojärvi, J., Wachsman, G., Prasad, K., Heidstra, R., and Scheres, B. (2014). PLETHORA gradient formation mechanism separates auxin responses. Nature **515,** 125-129.

Marhava, P., Hoermayer, L., Yoshida, S., Marhavý, P., Benková, E., and Friml, J. (2019). Re-activation of stem cell pathways for pattern restoration in plant wound healing. Cell **177,** 957-969.

Matsubayashi, Y., and Sakagami, Y. (1996). Phytosulfokine, sulfated peptides that induce the proliferation of single mesophyll cells of *Asparagus officinalis* L. Proc. Natl. Acad. Sci. USA **93,** 7623-7627.

Matsuoka, K., Sugawara, E., Aoki, R., Takuma, K., Terao-Morita, M., Satoh, S., and Asahina, M. (2016). Differential cellular control by cotyledon-derived phytohormones involved in graft reunion of Arabidopsis hypocotyls. Plant Cell Physiol. **57,** 2620-2631.

Mehrnia, M., Balazadeh, S., Zanor, M.-I., and Mueller-Roeber, B. (2013). EBE, an AP2/ERF transcription factor highly expressed in proliferating cells, affects shoot architecture in Arabidopsis. Plant Physiol. **162,** 842-857.

Melnyk, C.W., Gabel, A., Hardcastle, T.J., Robinson, S., Miyashima, S., Grosse, I., and Meyerowitz, E.M. (2018). Transcriptome dynamics at *Arabidopsis* graft junctions

reveal an intertissue recognition mechanism that activates vascular regeneration. Proc. Natl. Acad. Sci. USA **115,** E2447-E2456.

Miyashima, S., Roszak, P., Sevilem, I., Toyokura, K., Blob, B., Heo, J.-o., Mellor, N., Help-Rinta-Rahko, H., Otero, S., Smet, W., Boekschoten, M., Hooiveld, G., Hashimoto, K., Smetana, O., Siligato, R., Wallner, E.-S., Mähönen, A.P., Kondo, Y., Melnyk, C.W., Greb, T., Nakajima, K., Sozzani, R., Bishopp, A., De Rybel, B., and Helariutta, Y. (2019). Mobile PEAR transcription factors integrate positional cues to prime cambial growth. Nature **565,** 490-494.

Nakagami, H., Sekine, M., Murakami, H., and Shinmyo, A. (1999). Tobacco retinoblastoma-related protein phosphorylated by a distinct cyclin-dependent kinase complex with Cdc2/cyclin D *in vitro*. Plant J. **18,** 243-252.

Nakajima, K., Sena, G., Nawy, T., and Benfey, P.N. (2001). Intercellular movement of the putative transcription factor SHR in root patterning. Nature **413,** 307-311.

Nakano, T., Suzuki, K., Fujimura, T., and Shinshi, H. (2006). Genome-wide analysis of the ERF gene family in Arabidopsis and rice. Plant Physiol. **140,** 411-432.

Ohme-Takagi, M., and Shinshi, H. (1995). Ethylene-inducible DNA binding proteins that interact with an ethylene-responsive element. Plant Cell **7,** 173-182.

Papi, M., Sabatini, S., Altamura, M.M., Hennig, L., Schäfer, E., Costantino, P., and Vittorioso, P. (2002). Inactivation of the phloem-specific Dof zinc finger gene *DAG1* affects response to light and integrity of the testa of Arabidopsis seeds. Plant Physiol. **128,** 411-417.

Patro, R., Duggal, G., Love, M.I., Irizarry, R.A., and Kingsford, C. (2017). Salmon provides fast and bias-aware quantification of transcript expression. Nat. Methods **14,** 417-419.

Ramirez-Parra, E., Perianez-Rodriguez, J., Navarro-Neila, S., Gude, I., Moreno-Risueno, M.A., and del Pozo, J.C. (2017). The transcription factor *OBP4* controls root growth and promotes callus formation. New Phytol. **213,** 1787-1801.

Ricci, L., and Srivastava, M. (2018). Wound-induced cell proliferation during animal regeneration. Wiley Interdiscip. Rev.-Dev. Biol. **7,** e321.

Robinson, M.D., McCarthy, D.J., and Smyth, G.K. (2010). edgeR: a Bioconductor package for differential expression analysis of digital gene expression data. Bioinformatics **26,** 139-140.

Rueda-Romero, P., Barrero-Sicilia, C., Gómez-Cadenas, A., Carbonero, P., and Oñate-Sánchez, L. (2012). *Arabidopsis thaliana* DOF6 negatively affects germination in non-after-ripened seeds and interacts with TCP14. J. Exp. Bot. **63,** 1937-1949.

Sarkar, A.K., Luijten, M., Miyashima, S., Lenhard, M., Hashimoto, T., Nakajima, K., Scheres, B., Heidstra, R., and Laux, T. (2007). Conserved factors regulate signalling in *Arabidopsis thaliana* shoot and root stem cell organizers. Nature **446,** 811-814.

Sena, G., Wang, X., Liu, H.-Y., Hofhuis, H., and Birnbaum, K.D. (2009). Organ regeneration does not require a functional stem cell niche in plants. Nature **457,** 1150-1153.

Skirycz, A., Radziejwoski, A., Busch, W., Hannah, M.A., Czeszejko, J., Kwaśniewski, M., Zanor, M.-I., Lohmann, J.U., De Veylder, L., Witt, I., and Mueller-Roeber, B. (2008). The DOF transcription factor OBP1 is involved in cell cycle regulation in *Arabidopsis thaliana*. Plant J. **56,** 779-792.

Smet, W., Sevilem, I., de Luis Balaguer, M.A., Wybouw, B., Mor, E., Miyashima, S., Blob, B., Roszak, P., Jacobs, T.B., Boekschoten, M., Hooiveld, G., Sozzani, R., Helariutta, Y., and De Rybel, B. (2019). DOF2.1 controls cytokinin-dependent vascular cell proliferation downstream of TMO5/LHW. Curr. Biol. **29,** 520-529.

Soneson, C., Love, M.I., and Robinson, M.D. (2015). Differential analyses for RNA-seq: transcript-level estimates improve gene-level inferences. F1000Res. **4,** 1521.

Sussex, I.M. (2008). The scientific roots of modern plant biotechnology. Plant Cell **20,** 1189-1198.

Tian, C., Wan, P., Sun, S., Li, J., and Chen, M. (2004). Genome-wide analysis of the GRAS gene family in rice and *Arabidopsis*. Plant Mol. Biol. **54,** 519-532.

Torres-Galea, P., Hirtreiter, B., and Bolle, C. (2013). Two GRAS proteins, SCARECROW-LIKE21 and PHYTOCHROME A SIGNAL TRANSDUCTION1, function cooperatively in phytochrome A signal transduction. Plant Physiol. **161,** 291-304.

Torres-Galea, P., Huang, L.-F., Chua, N.-H., and Bolle, C. (2006). The GRAS protein SCL13 is a positive regulator of phytochrome-dependent red light signaling, but can also modulate phytochrome A responses. Mol. Genet. Genomics **276,** 13-30.

van den Berg, C., Willemsen, V., Hendriks, G., Weisbeek, P., and Scheres, B. (1997). Short-range control of cell differentiation in the *Arabidopsis* root meristem. Nature **390,** 287-289.

Van Leene, J., Eeckhout, D., Cannoot, B., De Winne, N., Persiau, G., Van De Slijke, E., Vercruysse, L., Dedecker, M., Verkest, A., Vandepoele, K., Martens, L., Witters, E., Gevaert, K., and De Jaeger, G. (2015). An improved toolbox to unravel the plant cellular machinery by tandem affinity purification of *Arabidopsis* protein complexes. Nat. Protoc. **10,** 169-187.

Van Leene, J., Han, C., Gadeyne, A., Eeckhout, D., Matthijs, C., Cannoot, B., De Winne, N., Persiau, G., Van De Slijke, E., Van de Cotte, B., Stes, E., Van Bel, M., Storme, V., Impens, F., Gevaert, K., Vandepoele, K., De Smet, I., and De Jaeger, G. (2019). Capturing the phosphorylation and protein interaction landscape of the plant TOR kinase. Nat. Plants **5,** 316-327.

van Wijk, K.J., Leppert, T., Sun, Q., Boguraev, S.S., Sun, Z., Mendoza, L., and Deutsch, E.W. (2021). The Arabidopsis PeptideAtlas: harnessing worldwide proteomics data to create a comprehensive community proteomics resource. Plant Cell **33,** 3421-3453.

Wachsman, G., Heidstra, R., and Scheres, B. (2011). Distinct cell-autonomous functions of *RETINOBLASTOMA-RELATED* in *Arabidopsis* stem cells revealed by the Brother of Brainbow clonal analysis system. Plant Cell **23,** 2581-2591.

Ward, J.M., Cufr, C.A., Denzel, M.A., and Neff, M.M. (2005). The Dof transcription factor OBP3 modulates phytochrome and cryptochrome signaling in Arabidopsis. Plant Cell **17,** 475-485.

Weimer, A.K., Nowack, M.K., Bouyer, D., Zhao, X., Harashima, H., Naseer, S., De Winter, F., Dissmeyer, N., Geldner, N., and Schnittger, A. (2012). Retinoblastoma related1 regulates asymmetric cell divisions in *Arabidopsis*. Plant Cell **24,** 4083-4095.

Wildwater, M., Campilho, A., Perez-Perez, J.M., Heidstra, R., Blilou, I., Korthout, H., Chatterjee, J., Mariconti, L., Gruissem, W., and Scheres, B. (2005). The *RETINOBLASTOMA-RELATED* gene regulates stem cell maintenance in *Arabidopsis* roots. Cell **123,** 1337-1349.

Xu, L., and Huang, H. (2014). Genetic and epigenetic controls of plant regeneration. Curr. Top. Dev. Biol. **108,** 1-33.

Zhang, A., Matsuoka, K., Kareem, A., Robert, M., Roszak, P., Blob, B., Bisht, A., De Veylder, L., Voiniciuc, C., Asahina, M., and Melnyk, C.W. (2022). Cell-wall damage activates DOF transcription factors to promote wound healing and tissue regeneration in *Arabidopsis thaliana*. In Curr. Biol.

Zhou, W., Lozano-Torres, J.L., Blilou, I., Zhang, X., Zhai, Q., Smant, G., Li, C., and Scheres, B. (2019). A jasmonate signaling network activates root stem cells and promotes regeneration. Cell **177,** 942-956.

FIGURES

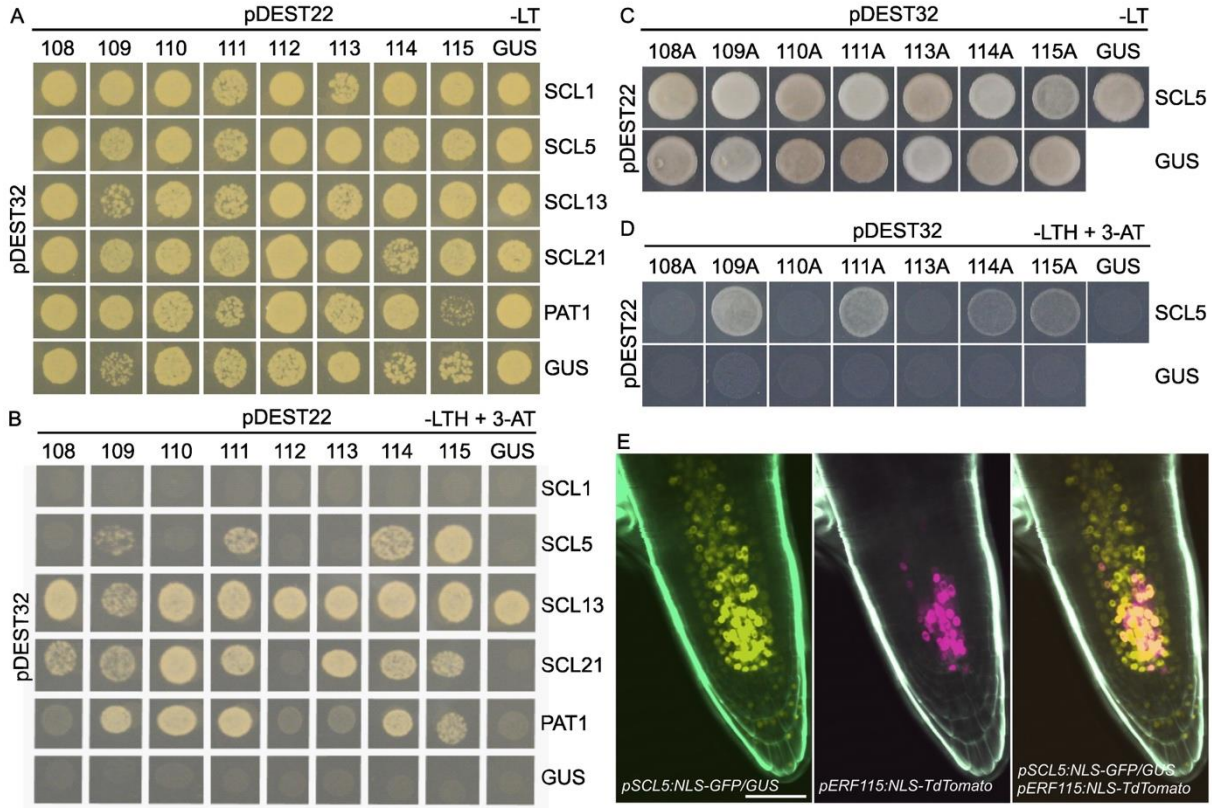

Figure 1. **SCL5 is an interaction partner of ERF115.** A and B, Yeast two-hybrid interactions between EREB-DREB subfamily X (cloned as prey in the pDEST22 vector) and PAT1 subfamily GRAS-domain (baits in the pDEST32 vector) transcription factors grown on medium holding (-LT) (A) or lacking histidine (-LTH) supplemented with 10 mM 3-AT (B). Interactions were scored by gain of histidine prototrophy. The GUS gene was taken along as a negative control. C and D, Yeast two-hybrid interactions between the newly annotated SCL5 (cloned as prey in the pDEST22 vector) and the N-terminal ERF A-fragments (baits in the pDEST32 vector) grown on medium holding (-LT) (C) or lacking histidine (-LTH) supplemented with 80 mM 3-AT (D). Interactions were scored by gain of histidine prototrophy. E, Confocal imaging of *SCL5* and *ERF115* expression in a root tip treated for 24 h with 0.6 µg/mL bleomycin. *pSCL5:NLS-GFP/GUS* (left), *pERF115:NLS-TdTomato* (middle), merge (right). All images were acquired at the same magnification; scale bar = 50 µm. Cell walls were counterstained using SCRI Renaissance 2200.

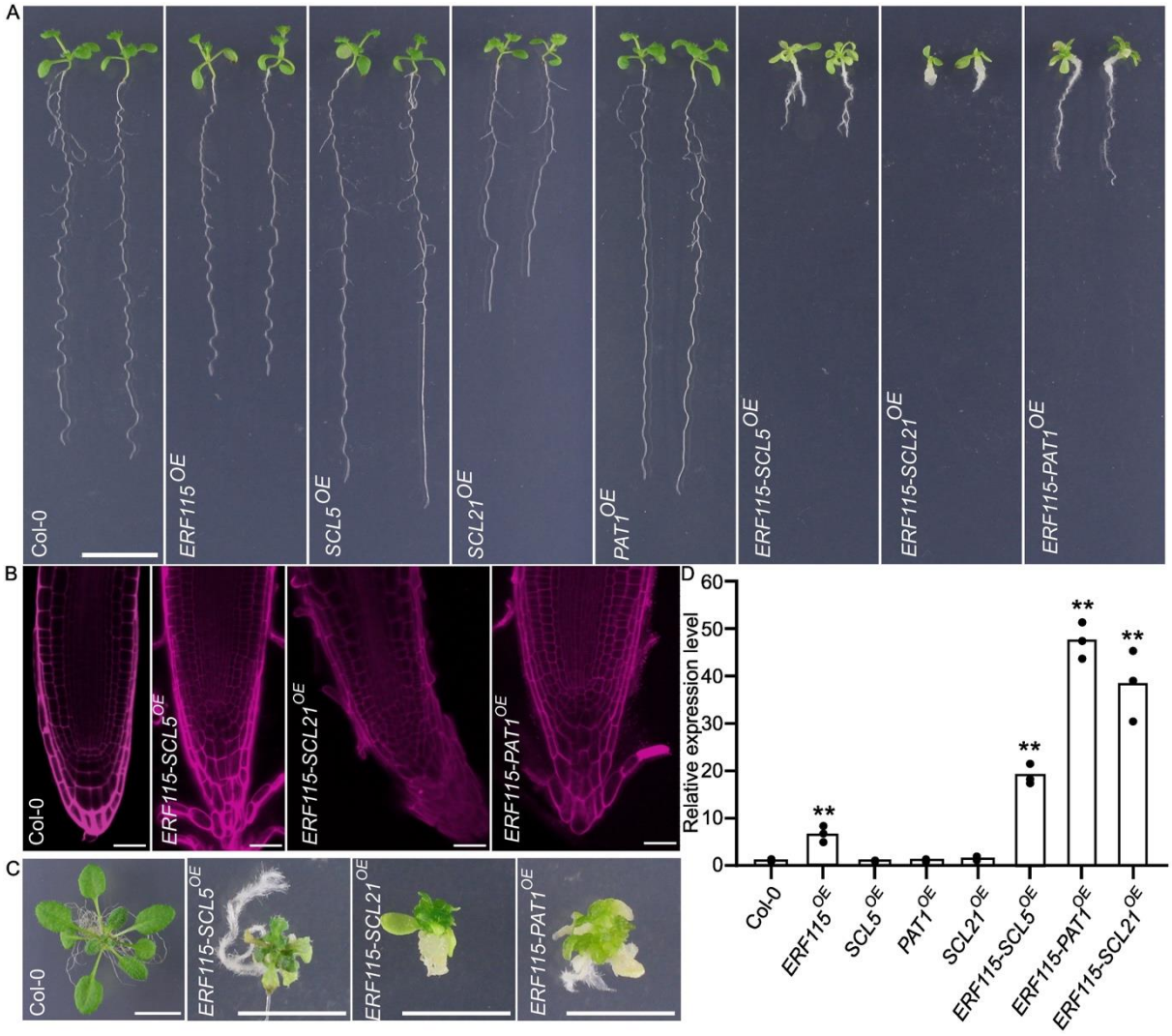

Figure 2. *ERF115-GRAS* ectopic co-overexpression activates hyperproliferation. A, Twelve-day-old wild-type, parental plants and F1 progeny plants resulting from a cross between *ERF115*^{OE} and respective *GRAS*^{OE} lines. All images were acquired at the same magnification; scale bar = 1 cm. B, Confocal images of 7-day-old root meristems of the *ERF115*^{OE}-*GRAS*^{OE} lines. Scale bars = 20 µm. Cell walls were counterstained using propidium iodide (PI). C, One-month-old control (Col-0) and *ERF115*^{OE}-*GRAS*^{OE} F1 plants. Scale bars = 1 cm. D, *PSK5* relative expression levels in control (Col-0) and *ERF115* and *GRAS* single and double overexpressors. Error bars indicate ± SEM (**P < 0.01, ANOVA followed by Tukey's multiple comparison test, n = 3 with each biological repeat holding > 3 seedlings).

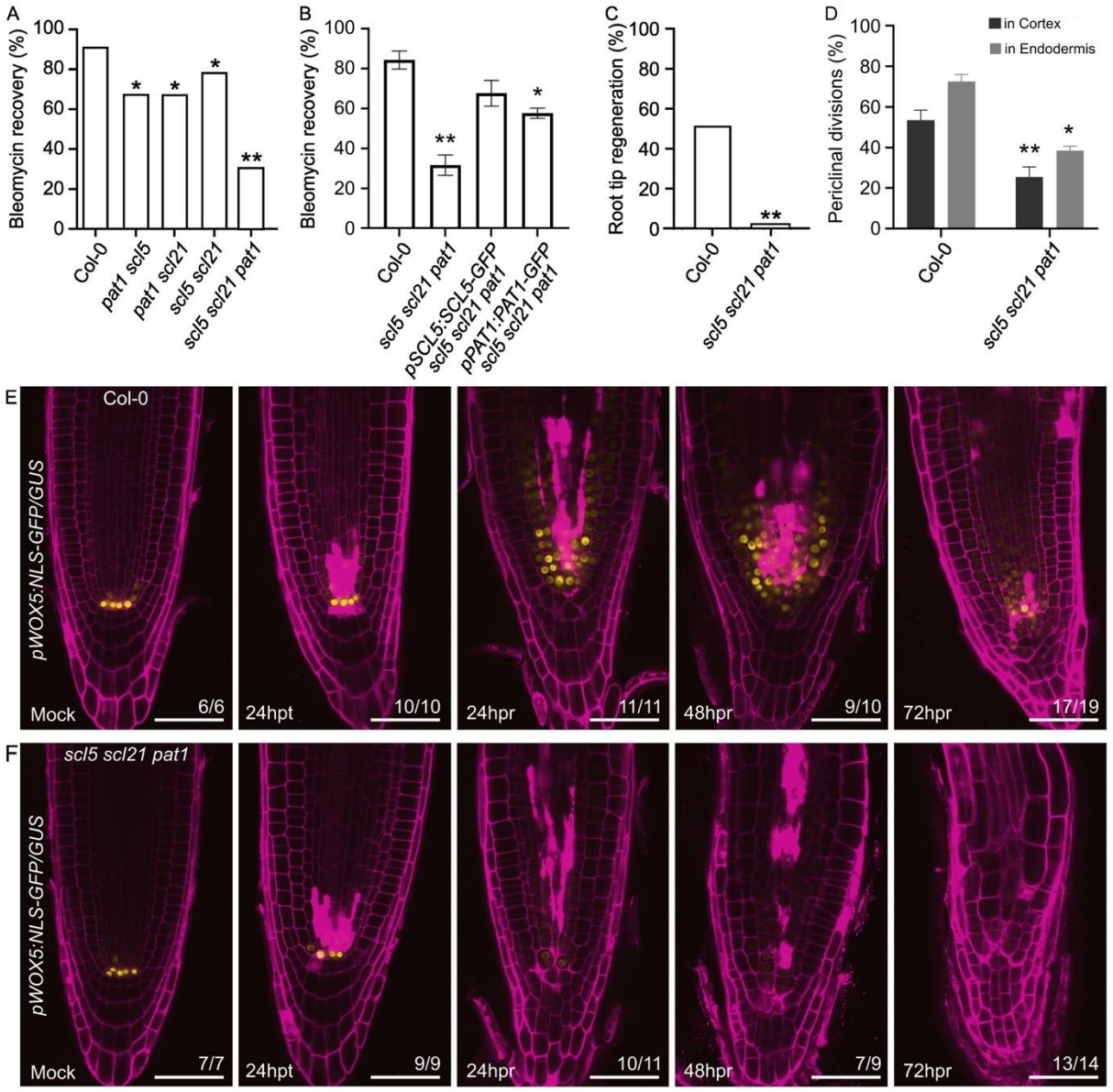

Figure 3. Triple mutant *scl5 scl21 pat1* plants are regeneration deficient. A, Recovery percentage following five days after a 24-h 0.6 µg/mL bleomycin treatment of the wild type (Col-0) and indicated higher order mutants. Recovery was scored defective by an arrested root growth and visual confirmation of a collapsed root meristem by confocal microscopy (*P < 0.05; **P < 0.001, Fisher's exact test, n > 80 evenly distributed over 3 biological repeats). B, Complementation of the *scl5 scl21 pat1* triple mutant using translational reporters of C-terminally GFP-tagged SCL5 and PAT1 proteins (*P < 0.05; **P < 0.001, Fisher's exact test, n > 80 evenly distributed over 3 biological repeats). C, Regeneration percentage following 72 h post root tip excision of wild-type (Col-0) and *scl5 scl21 pat1* triple mutant plants (**P < 0.001, χ^2 test, n > 75 evenly distributed over 3 biological repeats). D, Quantification of periclinal divisions in cortex and endodermis following ablation of epidermal and cortical cells in wild-type (Col-0) and *scl5 scl21 pat1* triple mutant plants (**P < 0.01; *P <0.05; Student's *t*-test, n

> 30 ablation events executed in at least 18 roots). E and F, *pWOX5:NLS-GFP/GUS* marker expression in wild-type (Col-0) (E) and *scl5 scl21 pat1* triple mutant (F) root meristems before treatment (Mock), 24 h post treatment (hpt) with 0.6 µg/mL bleomycin, and 24, 48 and 72 h post recovery (hpr) on bleomycin-free medium. Scale bars = 20 µm. Cell walls were counterstained using PI. The number of identical independent observations as shown within the respective representative images.

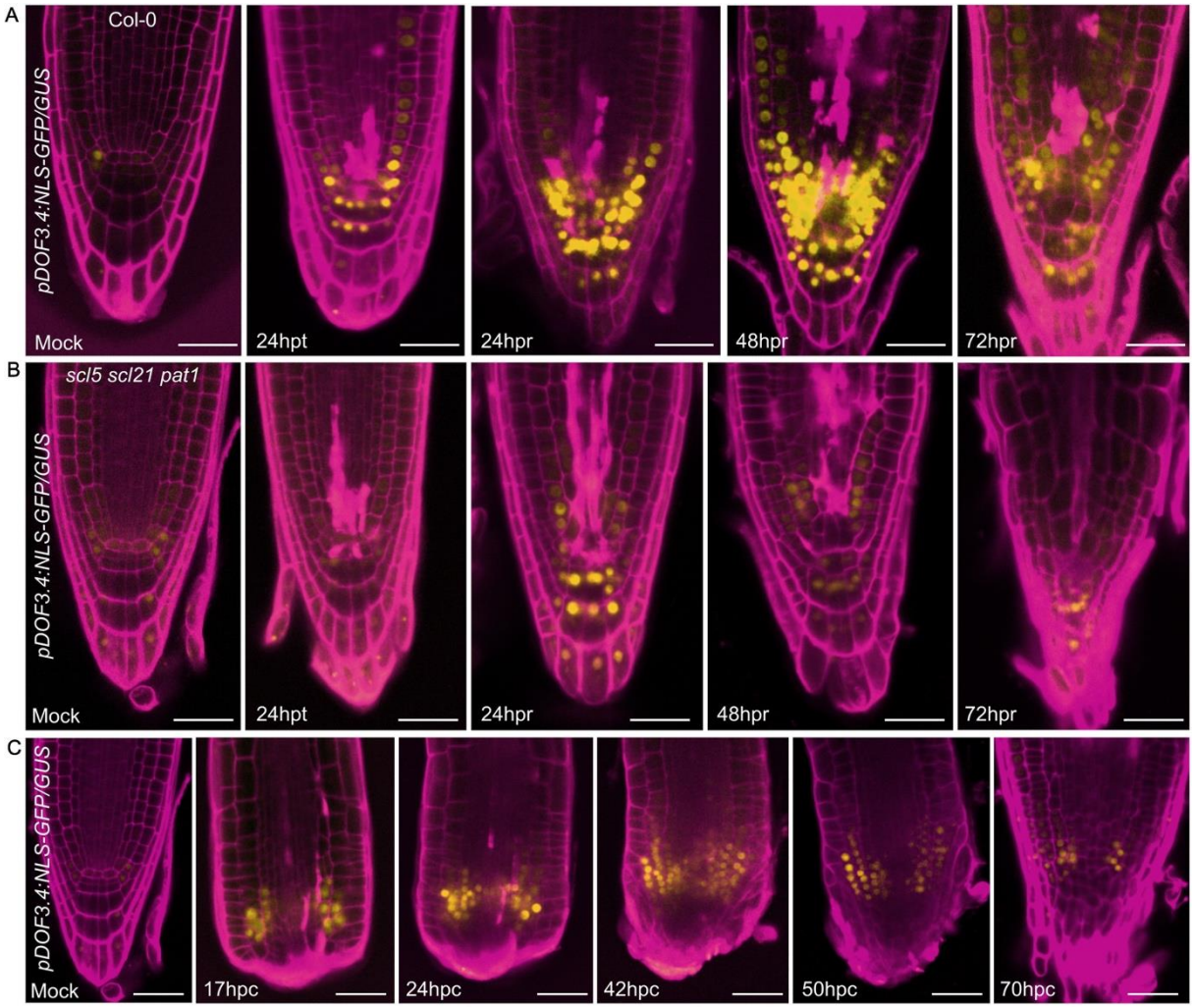

Figure 4. *DOF3.4* is a wound-responsive gene operating downstream of SCL5, SCL21 and PAT1. A and B, Expression pattern of *pDOF3.4:NLS-GFP/GUS* in control (Col-0) (A) and *scl5 scl21 pat1* triple mutant plants (B) before treatment (Mock), 24 h post treatment (hpt) with 0.6 µg/mL bleomycin, and 24, 48 and 72 h post recovery (hpr) on bleomycin-free medium. C, *pDOF3.4:NLS-GFP/GUS* (Col-0 background) during root tip regeneration at indicated h post cut (hpc). A-C, Cell walls were counterstained using PI. All images were acquired at the same magnification; scale bars = 20 µm.

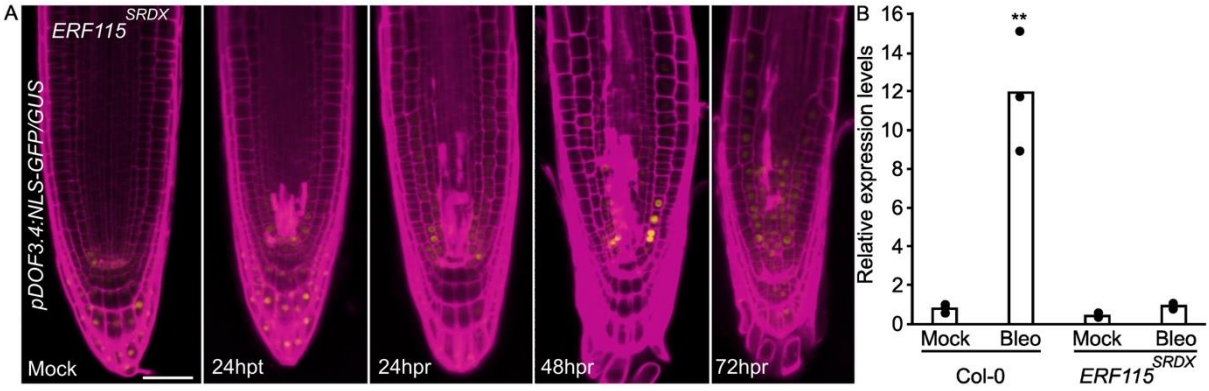

Figure 5. Bleomycin-induced *DOF3.4* expression is ERF115 dependent. A, *pDOF3.4:NLS-GFP/GUS* expression in the *ERF115*^{SRDX} mutant root meristem during the recovery process following bleomycin-induced stem cell death. All images were acquired at the same magnification; scale bar = 20 µm. Cell walls were counterstained using PI. B, Relative expression levels of *DOF3.4* measured by RT-qPCR in wild-type (Col-0) versus *ERF115*^{SRDX} root tips being either mock-treated or treated for 24 h with 0.6 µg/mL bleomycin. Data indicate mean ± s.e.m. (**P < 0.01, ANOVA followed by Tukey's multiple comparison test compared with control, n = 3 with each biological repeat holding > 100 root tips).

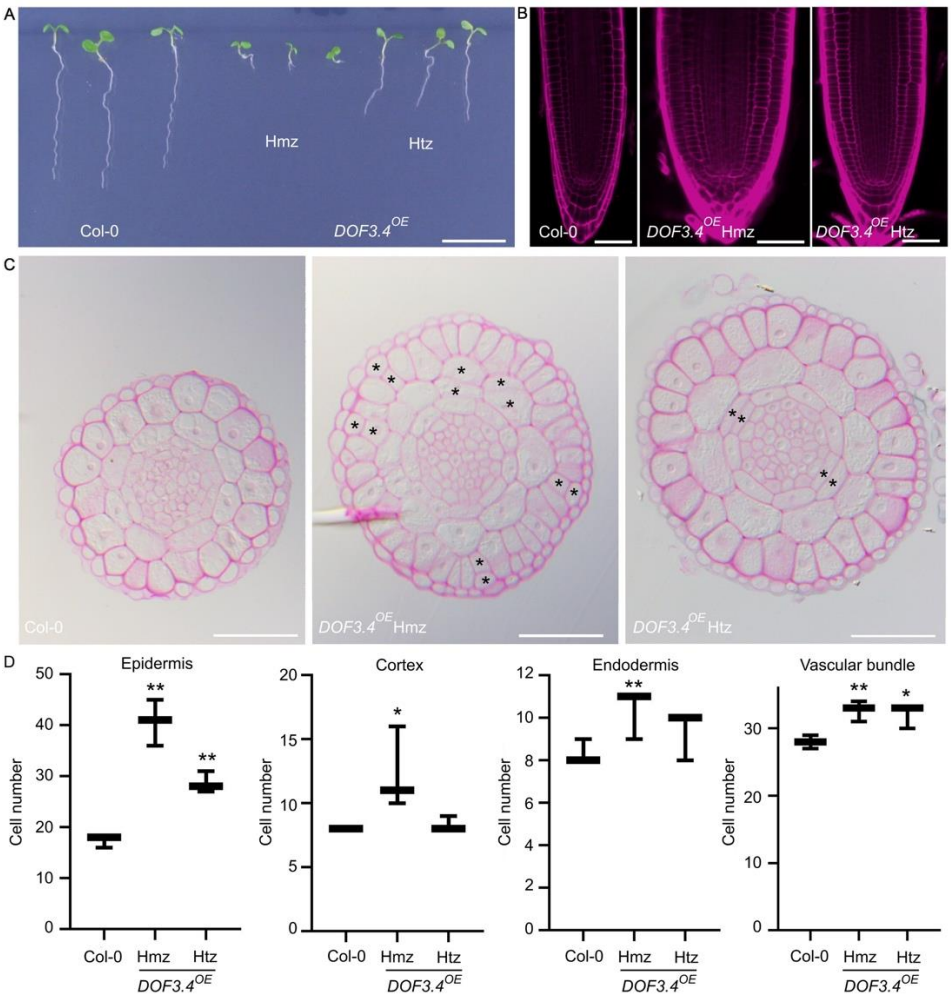

Figure 6. Ectopic *DOF3.4* expression activates periclinal cell divisions. A, Phenotypes of control (Col-0) and *DOF3.4* overexpression (*DOF3.4*^{OE}) homozygous (Hmz) and hemizygous (Htz) seedlings. Scale bar = 1 cm. B, Confocal images of control (Col-0) and *DOF3.4*^{OE} Hmz and Htz root meristems. Scale bars = 20 µm. Cell were counterstained using PI. C, Control (Col-0) and *DOF3.4*^{OE} Hmz and Htz root meristems showing periclinal divisions in epidermal, cortical and endodermal cell layers indicated by *. Root sectioning was performed on 5-day-old plants. Scale bars = 50 µm. D, Quantification of cell numbers in different cell layers in Col-0 and *DOF3.4*^{OE} plants (**$P < 0.01$, *$P < 0.05$, ANOVA followed by Tukey's multiple comparison test, n = 3).

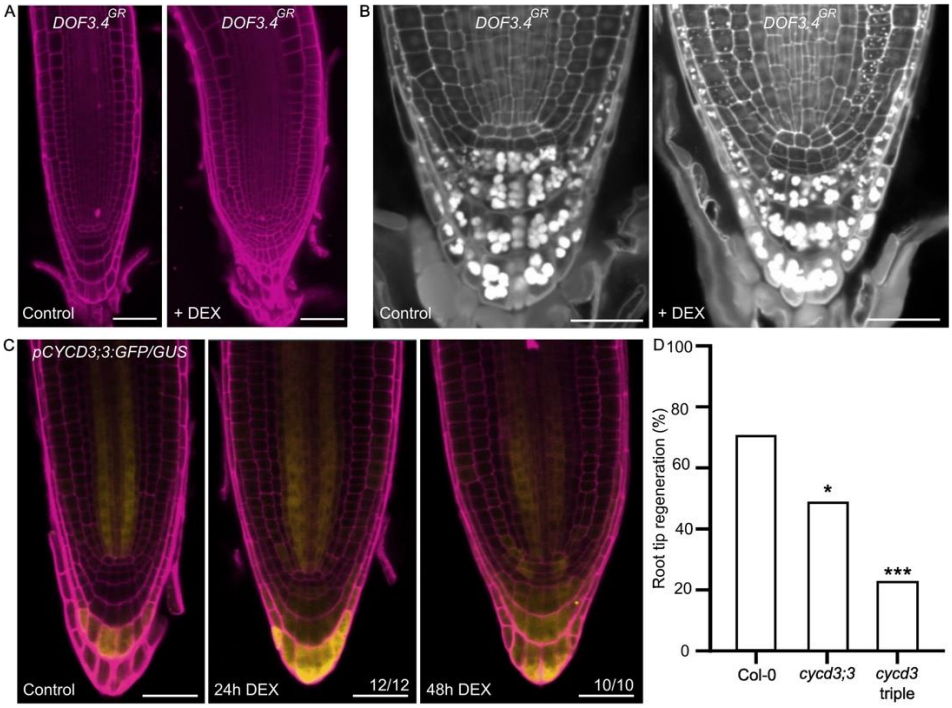

Figure 7. DOF3.4 activates *CYCD3;3* expression required for root tip regeneration. A, Confocal images of *DOF3.4*^{GR} root meristems in the absence (control) or presence (+) of 10 μM DEX (55 h treatment). Scale bars = 20 μm. Cell walls were counterstained using PI. B, Schiff staining of *DOF3.4*^{GR} meristems in the absence or presence of 10 μM DEX (55 h treatment). Scale bars = 50 μm. C, *pCYCD3;3:GFP/GUS* expression in *DOF3.4*^{GR} meristems in the absence and presence of 10 μM DEX (48 h treatment). Scale bars = 50 μm. Cell walls were counterstained using PI. Ratios at the right bottom indicate the number of identical observations. D, Regeneration percentage 72 h post root tip excision of the wild type (Col-0), and *cycd3;3* single and *cycd3;1 cycd3;2 cycd3;3* triple mutants (*cycd3*) (*$P < 0.01$; ***$P < 0.001$, Fisher's exact test, n > 75 evenly distributed over 3 biological repeats).

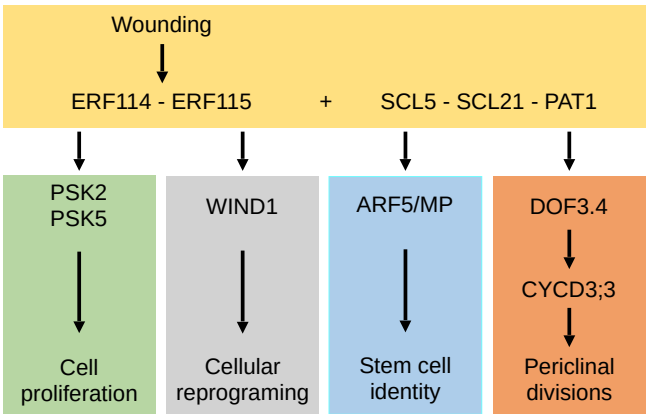

Figure 8. Model for ERF114/ERF115-mediated regeneration.

Wound-induced activation of ERF114 and ERF115 would result in the heterodimerization with the SCL5/SCL21/PAT1 transcription factors to activate the expression of PSK2/5, WIND1, ARF5/MP and DOF3.4 that promote cell proliferation, cellular reprograming, stem cell identity and periclinal cell division, respectively. DOF3.4 activates cell division through transcriptional activation of CYDD3;3.

Table 1. ERF115 FAST-IP data. List of significantly enriched proteins identified in ERF115 pull downs, as identified by LC-MS/MS on Q Exactive HF in GS^{TEV}-tagged ERF115 pull downs. Only proteins with at least two peptide sequences, identified in at least two out of three replicates, and enriched by quantitative analysis versus a large dataset of similar non-related bait pull down experiments were retained.

Protein accession	Protein description	# identified/3 experiments
AT5G07310	ERF115, Integrase-type DNA-binding superfamily protein	3
AT1G50600	SCL5 | scarecrow-like 5	3
AT1G74380	XXT5 | xyloglucan xylosyltransferase 5	3
AT2G04890	SCL21 | SCARECROW-like 21	3
AT2G44040	Dihydrodipicolinate reductase, bacterial/plant	3
AT3G59890	Dihydrodipicolinate reductase, bacterial/plant	3
AT3G62720	ATXT1, XT1, XXT1 | xylosyltransferase 1	3
AT5G13330	Rap2.6L (ERF113) | related to AP2 6l	3
AT5G61890	ERF114, Integrase-type DNA-binding superfamily protein	2

Table 2. Top-five upregulated genes in Col-0 only, post 24-h bleomycin treatment, identified following RNA-sequencing. FC (fold change) indicates ratio between Col-0 under treated (bleomycin) vs untreated condition.

Gene accession	Gene function	Fold change
AT4G24260	Endoglucanase 21/KOR3	202
AT1G15580	Auxin-responsive protein IAA5	133
AT3G50410	Dof zinc finger protein DOF3.4	79
AT1G20120	GDSL esterase/lipase	33
AT4G18910	Aquaporin NIP1-2	14